

KfK 2885
November 1979

The Velocity Distribution and Pressure Loss at Artificial Roughnesses with Sharp and Rounded Edges

L. Meyer, L. Vogel
Institut für Neutronenphysik und Reaktortechnik
Projekt Schneller Brüter

Kernforschungszentrum Karlsruhe

KERNFORSCHUNGSZENTRUM KARLSRUHE

Institut für Neutronenphysik und Reaktortechnik
Projekt Schneller Brüter

KfK 2885

The velocity distribution and pressure loss at
artificial roughnesses with sharp and rounded
edges

L. Meyer and L. Vogel

Kernforschungszentrum Karlsruhe GmbH, Karlsruhe

Als Manuskript vervielfältigt
Für diesen Bericht behalten wir uns alle Rechte vor

Kernforschungszentrum Karlsruhe GmbH
ISSN 0303-4003

Abstract

Measurements at two-dimensional roughnesses in a rectangular channel with air were performed in order to obtain information on the influence of rounded edges at artificial roughnesses on the velocity distribution and the momentum loss. A roughness with round edged trapezoidal ribs which is similar to the reference design for the Gas Cooled Fast Reactor, was compared with a sharp edged rectangular roughness of the same pitch-to-height ratio. The friction factor of the trapezoidal roughness is about 10% lower than that of the rectangular one. A systematic variation of the pitch to height ratio showed that the rectangular roughness had its maximum friction factor at the chosen pitch-to-height ratio, while the friction factor of the trapezoidal roughness could still be raised up to the value of the rectangular roughness by reducing the pitch.

The slope of the non-dimensional logarithmic velocity profile is less than $A_r = 2.5$ for both roughnesses if the origin of the profile is volumetrically defined. In order to obtain a slope of $A_r = 2.5$ the origin of the profile would have to be put behind the actual rough wall by $0.4 + 1.2$ rib heights.

Geschwindigkeitsverteilung und Druckverlust an künstlichen Rauigkeiten mit scharfen und abgerundeten Kanten

Zusammenfassung

Um den Einfluß von abgerundeten Kanten bei künstlichen Rauigkeiten auf Druckverlust und Geschwindigkeitsverteilung kennen zu lernen, wurden Messungen an zweidimensionalen Rauigkeiten im rechteckförmigen Plattenkanal mit Luft durchgeführt. Eine trapezförmige Rauigkeit mit abgerundeten Kanten, die der Referenzrauigkeit für den Gasgekühlten Schnellen Brüter ähnlich ist, wurde mit einer rechteckförmigen Rauigkeit gleichen Höhen-Abstandsverhältnisses verglichen. Der Reibungskoeffizient der trapezförmigen Rauigkeit liegt um ca. 10% unter dem der scharfkantigen Rauigkeit. Eine Parameterstudie zeigte jedoch, daß die scharfkantige Rauigkeit bei dem gewählten Rippenabstand ihren maximalen Reibungskoeffizienten besitzt, während durch eine Verringerung des Rippenabstandes bei der trapezförmigen Rauigkeit der Reibungskoeffizient auf den Wert der scharfkantigen Rauigkeit noch erhöht werden kann.

Die Steigung des dimensionslosen logarithmischen Geschwindigkeitsprofils liegt bei beiden Rauigkeiten unter dem Wert $A_r = 2.5$ bei volumetrischer Definition des Profilursprunges. Um eine Steigung von $A_r = 2.5$ zu erhalten, müßte der Ursprung des rauhen Profils um ca. 0.4 bis 1.2 Rauigkeitshöhen hinter die eigentliche Wand gelegt werden.

1. Introduction

For the augmentation of heat transfer in a Gas Cooled Fast Reactor artificial roughnesses at the surface of the fuel element rods have been proposed. The present reference design which was used in the BR2-calibration experiments /1/ is a two-dimensional roughness with round edged trapezoidal ribs. Rehme /2/ has measured the transport properties of turbulent flow at a similar roughness in a wall subchannel of a rod bundle. The wall shear stresses in this experiment had to be calculated with the assumption that the velocity profiles follow the 'law of the wall',

$$u^+ = A_r \ln \frac{y}{h} + R(h^+) \quad (1)$$

with a slope $A_r = 2.5$. The measurements at a single rough rod with trapezoidal ribs contained in a smooth tube for the determination of the heat transfer and friction coefficients of this roughness /3/ were evaluated by a method based on the same assumption /4,5/. However, measurements of the velocity profile at rectangular roughnesses /6-9/ yielded slopes A_r which deviated from the generally accepted value of $A_r = 2.5$, respectively 2.39.

Therefore the velocity distribution and the wall shear stress at a round edged trapezoidal roughness was measured in comparison with a sharp rectangular roughness of the same pitch-to-height ratio. The test section used in this investigation was the same as that used in earlier experiments /7,8/, which was a rectangular duct of sufficiently large aspect ratio for the flow along the mid-plane to be considered as that developed between parallel planes, simulating an annulus with a radius ratio close to one. Different relative roughness heights were obtained by altering the distance of the wide walls, of which one was carrying the roughnesses. The friction factor pertaining to the rough wall and the parameters A_r and R of the 'law of the rough wall' (1) were determined for Reynolds numbers high enough to be in the fully rough flow regime.

2. Experimental Setup

Since the test rig and measuring methods were described in great detail in reference /7/ and /8/ only the main features and modifications shall be described here.

The measurements were performed with air near the open outlet of a vertical rectangular channel (Fig.1). The internal dimensions of the channel are 700 mm in the wide direction (z) and 60 mm minimum and 210 mm maximum in the y-direction with tolerances of ± 0.5 mm. The roughness elements ($h=8.4$ mm) which were made of aluminum were fixed to one of the wide walls. 340 mm upstream of the outlet a roughness element was connected to a balance by which the force acting upon the rib was measured by means of a force transducer with 0.2 mm deflection at full range. The axial pressure drop was measured by 13 pressure taps (0.2 mm i.d.) in the smooth wide wall over a length of 6500 mm.

The velocities were measured by means of a circular Pitot tube with an outer diameter of 0.6 mm. The corresponding static pressures were measured with a second tube, axially aligned to the flow direction, which has four holes at its circumference and a ellipsoid shaped head. The lateral distance between static tube and Pitot tube was set to 10 mm. The wall shear stress at the smooth wall was determined by the Preston method, using the same Pitot tube and a static pressure tap in the smooth wall.

The cross slide, which was used to position the probes with an accuracy of 0.01 mm at any position of the flow cross section, was installed 150 mm downstream of the channel outlet in order not to block the flow. The probe support with a diameter of 4 mm at its end extended app. 300 mm into the channel, where the velocity measurements were taken.

The measuring technique and validity of the assumptions about the flow distribution had been tested extensively before and are discussed in detail in /7/.

Two roughnesses were investigated (Fig.2). The trapezoidal roughness has the same volume as the rectangular one. The channel width was varied four times for each roughness and four different mass flow rates were applied for each channel width.

p (mm)	p/h	h/b	$\frac{p-b}{h}$	h/L
90	10.71	0.28	7.14	0.14 0.099 0.062 0.04

The mean velocities were in the range between 14 and 28 m/s which resulted in a Reynolds number range of $10^5 < Re < 5 \cdot 10^5$.

3. Evaluation

The time mean velocity u was calculated with the differential pressure between Pitot tube and static tube and the density of the humid air. The position of the Pitot tube close to the smooth wall was corrected according to Mac Millan /10/. A correction of the velocities for the effect of turbulence was not applied.

The shear stress at the smooth wall was determined by Preston tubes using the Patel /11/ calibration. The shear stress at the rough wall was determined in two ways. The first method is based on the knowledge of the axial pressure drop dp/dx and the shear stress at the smooth wall τ_s . Since there is a region in the center of the channel in which the influence of the short side walls on the flow is negligible, a force balance of steady flow yields

$$(\tau_s + \tau_r) dzdx = L dzdp. \quad (2)$$

Because of the discrete roughnesses the average over one pitch must be taken at least, thus the mean shear stress is

$$\tau_r = L \frac{\Delta p}{\Delta x} - \tau_s \quad (3)$$

The reference surface of this shear stress is the smooth wall between the ribs ($\epsilon = 0$, see Fig.3). For another reference surface ($\epsilon \neq 0$) τ_r changes to

$$\tau_r = (L - \epsilon) \frac{\Delta p}{\Delta x} - \tau_s \quad (4)$$

The second method to determine the shear stress at the rough wall is based on the measurement of the force acting upon the rough wall.

Lavallee and Popovich /12/ showed that the negative and positive portions of the shear stress due to viscosity at the smooth wall between the ribs cancel each other out for square roughnesses with $p/h = 12.5$.

Thus, a force balance over the control volume with the length p and the height ϵ yields

$$F = \tau_r p + (p_1 - p_2) \epsilon. \quad (5)$$

Pressure patterns along the boundary of two successive grooves are assumed to be similar. From equation (5) the shear stress can be determined by

$$\tau_r = \frac{F}{p} - \frac{\Delta p}{\Delta x} \epsilon. \quad (6)$$

The dependence of τ_r on the choice of the reference surface (ϵ) is the same in equation (4) and (6).

The extension of the zones influenced by the smooth (\hat{y}_s) and rough (\hat{y}_r) wall respectively is given by the ratio of the wall shear stresses

$$\frac{\hat{y}_s}{\hat{y}_r} = \frac{\tau_s}{\tau_r} \quad (7)$$

With $\hat{y}_s = L - \hat{y}_r - \epsilon$, the length of the rough velocity profile is given by

$$\hat{y}_r = \frac{L - \epsilon}{1 + \tau_s / \tau_r} \quad (8)$$

This position of zero shear ($\tau=0$), however, is not dependent on ϵ which can be seen, if it is defined by \hat{y}_s . From equation (3) and (8) we get

$$\hat{y}_s = \frac{\tau_s}{\Delta p / \Delta x}. \quad (9)$$

4. Results

4.1 Axial velocity variation

Figure 4 shows the influence of the ribs on the velocity at a distance of $2h$ from the root of the ribs, at the position of maximum velocity and at the opposite smooth wall for the two lowest channel widths. The relative variation based on the average velocity at the respective y -position is greater at the smooth wall than that at the position of maximum velocity. All variations are greater for the trapezoidal ribs than for the square ribs, at the same channel width and Reynolds number. There are two axial positions, where the mean velocities can be measured. This is close to the upstream edge of the ribs and approximately at $x/h = 2 \div 3$ or $x/p = 0.2 \div 0.3$. This is somewhat different from the positions for square ribs, which were at $x/p = 0.31$ and $x/p = 0.88$ /7,8/.

4.2 Velocity profiles

Figures 5 and 6 show the velocity distributions for the maximum and minimum channel widths for both roughnesses. In the wide channel no distinct difference can be detected. In the narrow channel the effect of the axial traversing position is clearly to be seen, which is stronger for the trapezoidal roughness. The velocity profiles over rectangular roughnesses are more pointed than those over trapezoidal roughnesses.

The mean velocity profiles near the smooth surface are plotted in figure 7 - 10 in universal co-ordinates, together with a straight line representing the 'law of the smooth wall'

$$u^+ = A_s \ln y^+ + B \quad (10)$$

with $A_s = 2.5$ and $B = 5.5$.

The parameters A_s and B of the measured profiles were determined by a least square fit neglecting points for $y^+ < 70$ and those close to the maximum which do not fall upon a straight line. The mean values for each roughness and channel width combination are shown in figure 11, together with their variation, as function of the relative roughness height. The slopes A_s show a slight decrease with increasing roughness height while the parameter B increases. With the exception of the results for the widest channel width, there exists no remarkable difference between both roughnesses. The values of $A_s = 2.65$ for the wide channel and $A_s = 2.5$ for the narrow channel are the same as those for a square rib roughness with $p/h = 4$ on which was reported in reference /7/ and /8/. Also the B -values are approximately the same for the roughnesses.

The shear stresses at the rough wall, determined by equation (4) from the axial pressure drop and shear stress at the smooth wall, and by equation (6) from the force measurement at the rib, differed by less than $\pm 6\%$. For the evaluation of the friction velocity u_τ the average of both was used.

Figures 12 - 15 show the non-dimensional profiles at the rough wall together with a line representing the 'law of the rough wall' with a slope $A_r = 2.5$. The origin of the velocity profile is defined volumetrically, i.e. $\epsilon = h \cdot b/p$. There is no Reynolds number effect. Especially for the trapezoidal roughness in narrow channels the axial measuring position however has a distinctive effect on the velocity profile.

Figure 16 shows the slopes A_r and the roughness parameter R for all profiles. These values were obtained by a least square fit of the points lying upon a straight line neglecting those close to the roughness and to the maximum. There is some arbitraryness in this way of determination of A_r and R

and a variation of 0.2 in A_r is well within the scope. The profiles over the rectangular roughness have a slope close to $A_r = 2.0$ while the trapezoidal roughness gives slopes lower than that with a pronounced decrease with higher relative roughness heights. The corresponding R-values show a slight rise of approximately 0.5.

In order to obtain a slope of $A_r = 2.5$ the origin of the profile must be put behind the rough wall by 0.4 h (rib heights) for the rectangular, and by 1.2 h for the trapezoidal ribs. Figures 17 and 18 show the non-dimensional profiles with this definition of the origin for the maximum and minimum channel width. The corresponding parameters A_r and R determined by the same procedure as before are given in figure 19.

4.3 Integral quantities

4.3.1 Profile parameter

For the transformation of experiments in annuli and the calculation of friction factors from the logarithmic velocity profiles the profile parameters must be determined in a different way. The following conditions must be met:

$$\bar{u}_s = \frac{u_{rs}}{\hat{y}_s} \int_0^{\hat{y}_s} (A_s \ln y^+ + B) dy \quad (11)$$

$$\bar{u}_r = \frac{u_{rr}}{\hat{y}_r} \int_0^{\hat{y}_r} (A_r \ln \frac{Y}{h} + R) dy \quad (12)$$

$$u_{s_{max}} = u_{r_{max}} \quad (13)$$

Integration of equation (11) and (12) for the flow in a plane channel yields

$$\bar{u}_s = u_{\tau s} \left[A_s \ln \left(\frac{\hat{y}_s u_{\tau s}}{\nu} \right) + B - A_s \right] \quad (14)$$

$$\bar{u}_r = u_{\tau r} \left[A_r \ln \left(\frac{\hat{y}_r}{h} \right) + R - A_r \right] \quad (15)$$

and equation (13) reads

$$\left[A_s \ln \left(\frac{\hat{y}_s u_{\tau s}}{\nu} \right) + B \right] u_{\tau s} = \left[A_r \ln \left(\frac{\hat{y}_r}{h} \right) + R \right] u_{\tau r} \quad (16)$$

with $\hat{y}_r = L - \epsilon - \hat{y}_s$

The average velocities in the two zones were determined by numerical integration of the measured values between the respective walls and the zero shear stress line. At the rough wall the integration started at the rib tip or at the root depending on the measuring position. Of the five variables A_s, B, A_r and ϵ , two must be preset the other three are determined by equations (14), (15) and (16). A presetting of the parameters ϵ and B has turned out to be most suitable /7,8/.

For $B=5.5$ the resulting values of A_s are shown in figure 20. The scatter of these data is smaller than that of the least square fit data. With higher h/\hat{y}_r or h/\hat{y}_s respectively A_s decreases. The data can be correlated by

$$A_s = 2.60 - a_1 \ln \left(\frac{h/\hat{y}_r}{0.01} \right) \quad (17)$$

or

$$A_s = 2.55 + a_2 / \ln \left(0.1 \frac{h}{\hat{y}_s} \right) \quad (18)$$

with $a_1 = 0.06$ and $a_2 = 0.26$.

The drop of A_g with a rise of h/\hat{y}_r or h/\hat{y}_s is smaller than that found for square roughnesses /7,8/ where $a_1 = 0.1$ and $a_2 = 0.4$.

For the determination of the parameters A_r and R of the rough profile the origin ϵ of the profile must be defined. For the volumetric definition $\epsilon/h = b/p$ the results are shown in figure 21. Compared to the least square fit data of figure 16 the R -values are constant with varying h/\hat{y}_r , and the slopes A_r decrease steadily with increasing h/\hat{y}_r , stronger for the trapezoidal roughness than for the rectangular one. If a quasi-volumetric definition with $\epsilon/h = (b + \lambda_r/2)/p$ is applied, as proposed before /7,8/ ($\lambda_r/h=3$), the R values are raised slightly (fig.22).

The slopes A_r for the rectangular roughness are quite well described by the general correlation derived for square roughnesses

$$A_r = 2.5 + \frac{E}{\ln(h/\hat{y}_r)} \quad (19)$$

with $E = 2.3 - 0.026 \frac{p-b}{h}$. (20)

The slopes for the trapezoidal roughness are however lower, together with a higher R -value ($A_r=2.3+E/\ln(h/\hat{y}_r)$).

4.3.2 Friction factors

With the bulk velocities known from the numerical integration and the respective wall shear stresses, friction factors can be calculated:

$$\bar{u}_{r,s}^+ = \frac{\bar{u}_{r,s}}{(\tau_{r,s}/\rho)^{1/2}} \quad (21)$$

$$f_{r,s} = 2/\bar{u}_{r,s}^2 \quad (22)$$

The Reynolds numbers are given by

$$Re_{r,s} = \frac{\bar{u}_{r,s} \hat{y}_{r,s}}{\nu} \quad (23)$$

The theoretical friction factor of a smooth pipe at the same Reynolds number as that of the smooth and rough zone respectively were calculated by the relation of Prandtl-Nikuradse:

$$1/\sqrt{f_{o r,s}} = 4 \log (Re_{r,s} \sqrt{f_{o r,s}}) - 0.4 \quad (24)$$

The friction factor of the rough zone f_r over the relative roughness height h/L is shown in figure 23.

The friction factor of the trapezoidal roughness lies generally lower than that of the rectangular roughness by approximately 10%. A comparison of the friction factors for the trapezoidal roughness with other measurements is shown in table 1. Since these measurements were all taken in different geometrical flow channels a transformation to a common geometry is necessary. With the roughness parameters A_r and R the friction factor in a plane channel

$$\left(\frac{2}{f_r}\right)^{1/2} = A_r \ln \frac{\hat{y}}{h} + R - A_r \quad (25)$$

was determined for $\hat{y}/h = 0.05$.

An easy way to determine the roughness parameters A_r and R by the knowledge of the friction factors for different h/\hat{y}_r was suggested by Hodge et al /14/. Equation (25) can be written

$$\left(\frac{2}{f_r}\right)^{1/2} = A_r (\ln \frac{\hat{y}}{h} - 1) + R \quad (26)$$

From a plot $\left(\frac{2}{f_r}\right)^{1/2}$ over $(\ln \frac{\hat{y}}{h} - 1)$ the parameters A_r and R can be obtained (fig.24). This method implies however that both A_r and R are constant with varying h/\hat{y}_r . The resulting values $A_r = 1.9$ and $R = 6.1$ for the rectangular roughness agree

fairly well with those of figure 21. The R-value for the trapezoidal roughness is low by 0.45. Since the slope A_R determined by equations (14), (15) and (16) decreases with increasing relative roughness height h/\hat{y}_R , a constant slope of $A_R=1.9$ from figure 24 cannot be used for the determination of the zero shear stress line although it gives the right friction factors together with $R=6.55$. In order to obtain the true zero shear stress line with these values for A_R and R the parameters of the smooth profile would have to be changed. The slope A_S would have to vary between 3.0 and 3.8 and the parameter B between 2.3 and -2.3 for the trapezoidal roughness.

The effect of different profile parameters on the accuracy of the determination of the friction factors and zero shear stress line can be seen in table 2. Here the transformation was applied on the flow in the maximum and minimum channel width taking the bulk friction factor, the bulk Reynolds number and A_S and A_R as input. B was set to 5.5. The introduction of a variable slope A_S reduces the error by half. The results for a constant A_R , but lower than 2.5, lie between those with $A_S \neq 2.5$, $A_R = 2.5$, and the exact results. Which parameters are to be used must be decided as the circumstances may require.

Some authors use the ratio of the friction factor of the smooth zone with the smooth pipe friction factor f_s/f_{Os} for their transformation methods. Figures 25, 26, 27 and 28 show this ratio as function of f_r/f_{Or} , f_r/f_s , h/\hat{y}_R and h/\hat{y}_S respectively.

Within the range of scatter the results agree well with the correlations given by Warburton & Pirie /15/ (fig.25) and Warburton /16/ (fig.26).

The increase of f_s/f_{Os} with increasing h/\hat{y}_R is less than that found for square ribs (fig.27), which seems to confirm the trend found before for three dimensional roughnesses which caused an higher rise of f_s/f_{Os} . While the present roughnesses have a lower friction factor than square ribbed roughnesses, three dimensional ones had higher friction factors. If the ratio f_s/f_{Os} is plotted over h/\hat{y}_S (fig.28), the present results lie within the range of ± 0.03 of the equation found for square ribs /7,8/, however on the low side.

5. Friction factor variation with different pitch to height ratios

It is generally assumed that the optimum thermal performance is obtained by a roughness with a maximum friction factor. From former experiments with sharp edged rectangular roughnesses it is known that a ratio $(p-b)/h = 6 + 7$ yields the highest friction factor whereas for round edged ribs this ratio is not exactly known.

By means of a simple experiment the variation of the friction factor with a change of the pitch was investigated.

5.1 The Experiment

Ranga Raju & Garde /17/ had found, that the drag coefficient of two-dimensional strip roughnesses is constant after a distance of approximately $50 h$ from the first element irrespective of the roughness spacing, which means that the velocity close to the rough wall does not change any more. The velocity profile will not have adapted to the change in roughness in its full length after this relatively short distance, but it is assumed that the maximum velocity does not change much in the range of pitch to height ratios investigated. Measurements in a rough water channel in our laboratory with different entrance lengths have shown that the changes in the wall shear stress and velocity profile are small after a length of $2.5 L$ /18/.

So the pitch was changed only $60 h$ upstream and $40 h$ downstream of the measuring position, while the rest of the channel was fitted with the respective roughness with $p/h=10.71$. The channel width was kept at 210 mm . The reference velocities were measured with two Pitot tubes, the first at a position 700 mm upstream of the force measuring rib at the location of the maximum velocity (y_1), the other one close to the rough wall at a position downstream of the force measuring rib where the mean velocity across one pitch could be

be measured (y_2).

In addition to these velocities only the force at the rib was measured.

5.2 Evaluation

The wall shear stress is determined by

$$\tau_w = \frac{F}{p} \quad (27)$$

and a non-dimensional velocity can be formed

$$u^+ = \left(\frac{\tau_w}{\rho u^2} \right)^{1/2} \quad (28)$$

With two measured velocities lying upon the 'law of the rough wall' (1), which is assumed to be met close enough for the given task the slope A_r can be determined

$$A_r = (u_1^+ - u_2^+) / \ln \left(\frac{y_1}{y_2} \right) \quad (29)$$

The non-dimensional velocity at the rib tip u_h^+ is

$$u_h^+ = R = u_k^+ - A_r \ln \left(\frac{y_k}{h} \right) \quad (30)$$

Now a friction factor can be determined

$$\left(\frac{2}{f_r} \right)^{1/2} = A_r \ln \left(\frac{y_k}{h} \right) + R - A_r \quad (31)$$

Because of the shortcomings of the experiment this friction factor is not exact, but it is thought to be suited for the purpose of relative comparison.

5.3 Results

Figure 29 shows the friction factor f_r as function of the pitch to height ratio p/h for both roughnesses. It is a surprising result that the round edged roughness can reach the same friction factor as the sharp edged one, if the pitch is reduced. For a better understanding of this fact some additional measurements at single ribs concerning the drag coefficient and the length of the eddy zone downstream of a rib were performed. The drag coefficient related to the average velocity over the rib height was found to be $C_D = 0.9$ for the rectangular rib and $C_D = 0.6$ for the trapezoidal rib. These values were obtained by extrapolating measurements at different channel heights L to $h/L=0$. The length of the recirculating zone or reattachment length ℓ_r is shorter for the trapezoidal ribs with $\ell_r/h=4.2$ than that of the rectangular rib with $\ell_r/h=5.0$. This might explain the fact that the trapezoidal roughness reaches the maximum friction factor at a lower p/h -ratio. It remains to be seen whether the thermal performance of both types of roughnesses are the same also.

6. Conclusions

Measurements of the velocity distribution in a rectangular channel with one rough wall composed of two dimensional rectangular and round edged trapezoidal ribs were performed. The slopes of the nondimensional velocity profiles were found to be lower than 2.5 in both cases if the origin was defined volumetrically. A slope of $A_r=2.5$ is reached if the origin is put behind the rough wall, by $0.4 h$ for the rectangular roughness and by $1.2 h$ for the trapezoidal one. The parameters A_r and R were determined integrally for the use in a transformation method. For the rectangular roughness A_r can be described by a correlation which was derived from measurements at square roughnesses. For the trapezoidal roughness A_r is lower.

The friction factors of the trapezoidal roughness are lower by 10% than those of the rectangular one, it can however be raised to the same value if the pitch is reduced.

Nomenclature

- A slope of the logarithmic velocity profile
- B constant of the logarithmic velocity profile at smooth walls;
- b width of the roughness rib (m)
- d_h hydraulic diameter (m)
- E parameter of the velocity profile at the rough wall
- F force upon a roughness rib per unit length (Nm^{-1})
- f friction factor = $2\tau/\rho u^2$
- f_o friction factor of a smooth tube
- h height of roughness rib (m)
- h^+ dimensionless height of roughness rib = $h u_\tau/\nu$
- L width of channel (m)
- ℓ_r length of eddy downstream of a rib (reattachment length) (m)
- p axial pitch of the repeated roughness ribs (m)
- p pressure (Nm^{-2})
- u mean velocity (ms^{-1})
- u_τ friction velocity = $(\tau/\rho)^{1/2}$ (ms^{-1})
- u^+ dimensionless velocity = u/u_τ
- u average velocity in a section (ms^{-1})
- R parameter of the logarithmic velocity profile at rough walls

Re	Reynolds number = ud_h/ν
x	axial distance
y	distance normal to the wall
y^+	dimensionless distance from the wall = yu_τ/ν
\hat{y}	position of the zero shear stress line, length of respective zones
z	distance parallel to the wall normal to the flow

Greek symbols

ϵ	displacement of the origin of the velocity profile at rough walls (m)
ν	kinematic viscosity (m^2s^{-1})
ρ	density (kgm^{-3})
τ	shear stress (Nm^{-2})

Subscripts

m	mean value of a periodic quantity
max	maximum
dyn	dynamic
r	at the rough wall or pertaining to the rough zone
s	at the smooth wall or pertaining to the smooth zone
st	static
vol	volumetric definition of origin of velocity profile

References:

- /1/ M. Dalle Donne, J. Marek, A. Martelli, K. Rehme:
BR2 bundle mockup heat transfer experiments, Nuclear
Engineering and Design, Vol 40. No.1
pp. 143-156 (1977)
- /2/ K. Rehme:
The structure of turbulent flow through a wall subchannel
of a rod bundle with roughened rods, KfK-Bericht 2716 (1978)
- /3/ M. Dalle Donne, M. Hudina, M. Huggenberger, L. Meyer,
K. Rehme:
EIR, KfK joint heat transfer experiment on a single rod,
roughened with trapezoidal rounded ribs and cooled by
various gases, KfK-Bericht Nr. 2674 (1978)
- /4/ M. Dalle Donne:
Wärmeübergang von rauhen Oberflächen, KfK-Bericht Nr. 2397
(1977)
- /5/ M. Dalle Donne, L. Meyer:
Turbulent convective heat transfer from rough surfaces
with two-dimensional rectangular ribs, Int. J. Heat Mass
Transfer 20,6,583-620 (1977)
- /6/ W. Baumann:
Geschwindigkeitsverteilung bei turbulenter Strömung an
rauhem Wänden, KfK-Bericht Nr. 2618 (1978) und
Nr. 2680 (1978)
- /7/ L. Meyer:
Turbulente Strömung an Einzel- und Mehrfachrauigkeiten
im Plattenkanal, KfK-Bericht Nr. 2764 (1979)
- /8/ L. Meyer:
Pressure and velocity distribution in a plane channel
having one or two rough walls.
OECD-NEA, 5th Specialists Meeting on GCFR heat transfer,
Würenlingen, Schweiz (1979)

- /9/ F.P. Berger and A.W. Whitehead:
Fluid flow and heat transfer in tubes with internal square rib roughening, J.Br.Nucl. Energy Soc. 16, 2, 153-160 (1977)
- /10/ F.A. Mac Millan:
Experiments on Pitot-tubes in shear flow, ARC RM No.3028, London (1956)
- /11/ V.C. Patel:
Calibration of the Preston tube and limitation on its use in pressure gradients, J. Fluid Mechanics, 23 (1), 185-208 (1965)
- /12/ H.C. Lavallee and A.T. Popovich:
Fluid flow roughness elements investigated by photolysis method, Chem. Engng. Sci. 29, 49-59 (1974).
- /13/ K. Rehme:
Evaluation of the fluid-dynamic experiments with a rod bundle of 12 rods (MOL calibration experiments)
Report KfK 1276/1, p. 127 - 1/5 (1976) (in German)
- /14/ S.A. Hodge, J.P. Sanders, J.C. Conklin:
Determination of the Slope and Intercept of the Universal Velocity Profile from Pressure loss Measurements,
OECD-NEA Coordinating Group on Gas-cooled Fast Reactor Development 5th GCFR Heat Transfer Specialist Meeting
CFTL 79-51, (1979)
- /15/ C. Warburton, M.A.M. Pirie:
An improved method for analysing heat transfer and pressure drop tests on roughened rods in smooth channels
CEGB RD/B/N 2621, Berkely Nucl. Labs. (1973)
- /16/ C. Warburton:
The interpretation of tests on roughened pins in rough channels and the predication of cluster pressure drop from single-pin data,
CEGB RD/B/N 2930, Berkely Nucl. Labs. (1974)

/17/ K.G. Ranga Raju, R.J. Garde:

Resistance to flow over two-dimensional strip roughness,
J. Hydraulic. Div. Am. Soc. Civ. Engrs. 96 (HY3), 815-835
(1970)

/18/ H. Schalk, K. Rehme:

personal communication, Institut für Neutronenphysik
und Reaktortechnik, Kernforschungszentrum Karlsruhe

author	fluid	p/h	$\frac{p-b}{h}$	h/b	A_r	R	h/\hat{y}_r	$f_r(h/\hat{y}=0.05)$	
REHME /13/	air	10.84	6.91	0.255	2.5	5.55	0.059	0.01801	rod bundle
DALLE DONNE et al. /3/	CO ₂ He N ₂ air	10.84	6.91	0.255	2.5	5.4 6.2 6.4 5.3	0.025	0.02004 0.01597 0.01542 0.1889	annulus
REHME /2/	air	11.57	7.44	0.242	2.5 2.5	6.2±7.2 6.13	0.034±0.117	0.01597±0.01346 0.01618	wall subchannel of rod bundle: from velocity profile from axial pressure drop
this work	air	10.71	7.14	0.280	1.665 1.9	7.0 6.55	0.05	0.01880 0.01870	parallel plates

Table 1

h/L	A_S	A_R	R	$\Delta f_S (\%)$	$\Delta f_R (\%)$	$\Delta h/\hat{y}_R (\%)$
0.040	2.43	1.70	7.01	-	-	-
	2.43	1.90	6.60	-0.66	0.26	0.50
	2.43	2.50	5.40	-2.49	1.22	2.02
	2.50	2.50	5.34	-5.57	1.90	1.16
0.14	2.39	1.20	7.06	-	-	-
	2.39	1.90	6.50	-3.34	1.05	1.80
	2.39	2.50	6.02	-5.83	2.34	3.37
	2.50	2.50	5.96	-10.18	3.05	2.30

Table 2: Comparison of friction factors evaluated with different profile parameters for the trapezoidal roughness

Nr	h/L	\hat{y}_s/L	\hat{y}_r/L	h^+	ϵ/h	least square fit				f_s	Re_{s-3} 10^{-3}	f_r	Re_{r-3} 10^{-3}	f_r/f_s	f_r/f_{or}	f_s/f_{os}	
						A_r	R	A_s	B								
1Z	.140	.162	.838	1247	0.333	1.90	6.26	2.51	5.40	.00589	44	.0349	215	5.93	9.05	1.098	rectangular ribs
2Z	.140	.159	.841	1451	0.333	1.92	6.27	2.55	5.14	.00572	51	.0346	252	6.06	9.26	1.099	
3Z	.140	.167	.833	1012	0.333	1.90	6.30	2.45	5.76	.00612	37	.0350	173	5.71	8.70	1.096	
4A	.140	.165	.835	1254	0.333	1.77	6.59	2.51	5.23	.00592	45	.0373	209	6.30	9.61	1.111	
5Z	.099	.161	.839	1373	0.333	1.93	6.12	2.70	4.48	.00509	75	.0299	368	5.87	8.58	1.065	
6Z	.099	.167	.833	1117	0.333	1.95	6.08	2.53	5.30	.00535	63	.0302	296	5.64	8.32	1.079	
7Z	.099	.161	.839	1592	0.333	1.97	6.07	2.53	5.29	.00500	87	.0298	428	5.96	8.80	1.081	
8A	.099	.162	.838	1374	0.333	1.80	6.36	2.63	4.73	.00515	75	.0314	359	6.09	8.97	1.078	
9Z	.062	.177	.823	1156	0.333	2.14	5.85	2.64	4.75	.00453	125	.0241	546	5.32	7.44	1.054	
10Z	.062	.173	.827	1371	0.333	2.13	5.82	2.68	4.38	.00441	146	.0243	647	5.51	7.74	1.059	
11Z	.062	.183	.817	1015	0.333	2.16	5.88	2.65	4.65	.00461	115	.0235	481	5.11	7.10	1.056	
12A	.062	.181	.819	1143	0.333	2.11	5.97	2.63	4.63	.00456	127	.0243	535	5.32	7.46	1.066	
13Z	.040	.192	.808	1003	0.333	2.04	5.91	2.67	4.08	.00422	201	.0200	800	4.74	6.60	1.080	
14Z	.040	.190	.810	748	0.333	2.04	5.87	2.70	4.60	.00428	147	.0201	596	4.71	6.31	1.029	
15Z	.040	.189	.811	884	0.333	1.98	5.93	2.73	4.22	.00417	174	.0203	703	4.85	6.54	1.039	
16A	.040	.188	.812	884	0.333	1.98	5.95	2.64	4.69	.00423	171	.0206	699	4.86	6.64	1.050	
17Z	.140	.161	.839	1386	0.333	1.45	6.98	2.51	5.33	.00576	49	.0316	252	5.48	8.45	1.101	trapezoidal ribs
18Z	.140	.155	.845	1719	0.333	1.42	7.05	2.56	5.16	.00549	59	.0311	317	5.66	8.69	1.091	
19Z	.140	.158	.842	1554	0.333	1.43	7.03	2.52	5.33	.00562	54	.0312	285	5.55	8.54	1.098	
20A	.140	.159	.841	1584	0.333	1.20	7.60	2.53	5.14	.00566	56	.0330	279	5.94	9.18	1.111	
21Z	.099	.166	.834	1501	0.333	1.59	6.98	2.60	4.80	.00503	86	.0265	425	5.27	7.82	1.084	
22Z	.099	.169	.831	1377	0.333	1.62	6.97	2.67	4.42	.00511	81	.0264	389	5.17	7.67	1.087	
23Z	.099	.164	.836	1696	0.333	1.57	7.02	2.62	4.68	.00493	97	.0263	484	5.34	7.95	1.089	
24A	.099	.169	.831	1521	0.333	1.38	7.50	2.56	5.01	.00502	90	.0275	422	5.48	8.09	1.092	
25Z	.062	.180	.820	1243	0.333	1.89	6.66	2.71	4.21	.00444	140	.0216	617	4.88	6.83	1.057	
26Z	.062	.179	.821	1446	0.333	1.87	6.71	2.69	4.28	.00435	163	.0215	721	4.95	6.98	1.067	
27Z	.062	.184	.816	1092	0.333	1.90	6.59	2.64	4.61	.00459	125	.0219	536	4.78	6.75	1.068	
28A	.062	.185	.815	1212	0.333	1.91	6.73	2.64	4.53	.00446	141	.0220	592	4.94	6.91	1.066	
29Z	.040	.201	.799	851	0.333	1.80	6.75	2.57	4.84	.00426	183	.0185	697	4.35	5.97	1.071	
30Z	.040	.194	.806	966	0.333	1.77	6.71	2.65	4.45	.00415	199	.0187	793	4.52	6.18	1.059	
31Z	.040	.192	.808	726	0.333	1.79	6.62	2.65	5.00	.00426	145	.0191	592	4.48	5.98	1.022	
32A	.040	.200	.800	812	0.333	1.76	6.78	2.54	4.94	.00434	172	.0191	655	4.42	6.11	1.077	

Table 3: Results evaluated with volumetric definition of origin of the velocity profile

Nr	h/L	h/ \hat{y}_r	h/ \hat{y}_s	Re 10^{-3}	f	u	u_r	u_s/u_r	B=5.5 eq. (14-16)			$A_r=2.5$ eq. (14-16)			
									A_s	A_R	R	R	A_s	B	
1Z	.140	.175	0.908	130	.02035	17.96	17.76	1.070	2.39	1.58	6.40	6.16	3.12	1.55	rectangular ribs
2Z	.140	.175	0.923	151	.02013	20.78	20.55	1.070	2.35	1.57	6.43	6.18	3.14	1.35	
3Z	.140	.176	0.880	105	.02051	14.33	14.17	1.070	2.40	1.61	6.38	6.16	3.05	2.05	
4A	.140	.176	0.891	127	.02149	17.37	17.05	1.115	2.37	1.89	5.93	5.92	2.39	5.41	
5Z	.099	.122	0.634	222	.01746	21.38	21.17	1.061	2.45	1.57	6.44	6.08	3.19	1.14	
6Z	.099	.123	0.610	180	.01774	17.15	16.96	1.065	2.42	1.62	6.37	6.05	3.05	1.89	
7Z	.099	.122	0.637	258	.01737	24.78	24.52	1.067	2.42	1.61	6.42	6.09	3.09	1.49	
8A	.099	.122	0.631	217	.01822	20.81	20.53	1.085	2.42	1.74	6.06	5.89	2.78	3.41	
9Z	.062	.077	0.360	335	.01428	19.75	19.51	1.069	2.46	1.77	6.35	6.14	2.75	3.71	
10Z	.062	.077	0.366	396	.01433	23.61	23.31	1.076	2.45	1.81	6.24	6.10	2.65	4.20	
11Z	.062	.078	0.347	298	.01405	17.87	17.65	1.070	2.46	1.81	6.40	6.26	2.65	4.31	
12A	.062	.078	0.352	331	.01437	19.99	19.70	1.082	2.44	1.89	6.13	6.12	2.45	5.41	
13Z	.040	.050	0.211	501	.01208	18.93	18.71	1.061	2.41	1.78	6.45	6.22	2.65	3.87	
14Z	.040	.050	0.213	371	.01219	14.03	13.89	1.052	2.50	1.73	6.52	6.18	2.86	3.21	
15Z	.040	.050	0.214	439	.01219	16.68	16.48	1.064	2.48	1.84	6.27	6.15	2.61	4.66	
16A	.040	.050	0.216	435	.01238	16.67	16.49	1.060	2.46	1.78	6.31	6.07	2.72	3.79	
17Z	.140	.175	0.912	150	.01868	20.93	20.84	1.026	2.39	1.25	7.02	6.54	3.86	-2.61	trapezoidal ribs
18Z	.140	.174	0.948	188	.01829	25.90	25.83	1.019	2.40	1.18	7.13	6.59	4.08	-3.99	
19Z	.140	.174	0.927	170	.01839	23.50	23.42	1.022	2.39	1.21	7.10	6.59	3.97	-3.33	
20A	.140	.175	0.922	168	.01962	23.07	22.85	1.061	2.37	1.50	6.59	6.29	3.28	0.38	
21Z	.099	.122	0.617	256	.01577	25.05	24.96	1.023	2.41	1.27	7.29	6.60	3.82	-2.92	
22Z	.099	.123	0.605	235	.01576	22.59	22.49	1.026	2.41	1.31	7.26	6.62	3.71	-2.23	
23Z	.099	.122	0.624	290	.01562	28.05	27.94	1.023	2.40	1.26	7.35	6.63	3.84	-3.26	
24A	.099	.123	0.605	256	.01622	24.50	24.27	1.056	2.40	1.56	6.83	6.45	3.16	0.90	
25Z	.062	.077	0.353	378	.01303	22.54	22.40	1.035	2.45	1.49	7.29	6.65	3.33	-0.12	
26Z	.062	.077	0.355	442	.01292	27.07	26.89	1.038	2.44	1.51	7.30	6.68	3.28	-0.03	
27Z	.062	.078	0.346	330	.01325	20.25	20.11	1.036	2.44	1.50	7.22	6.60	3.27	0.23	
28A	.062	.078	0.344	367	.01324	22.51	22.27	1.058	2.44	1.71	6.87	6.58	2.84	2.95	
29Z	.040	.051	0.202	440	.01137	16.83	16.68	1.046	2.43	1.70	7.03	6.63	2.83	2.79	
30Z	.040	.050	0.209	496	.01144	19.22	19.06	1.044	2.45	1.65	7.04	6.55	2.95	2.13	
31Z	.040	.050	0.211	369	.01167	14.31	14.22	1.034	2.52	1.57	7.11	6.45	3.19	1.17	
32A	.040	.051	0.202	413	.01173	16.14	15.98	1.051	2.42	1.74	6.78	6.45	2.75	3.34	

Table 3 cont.

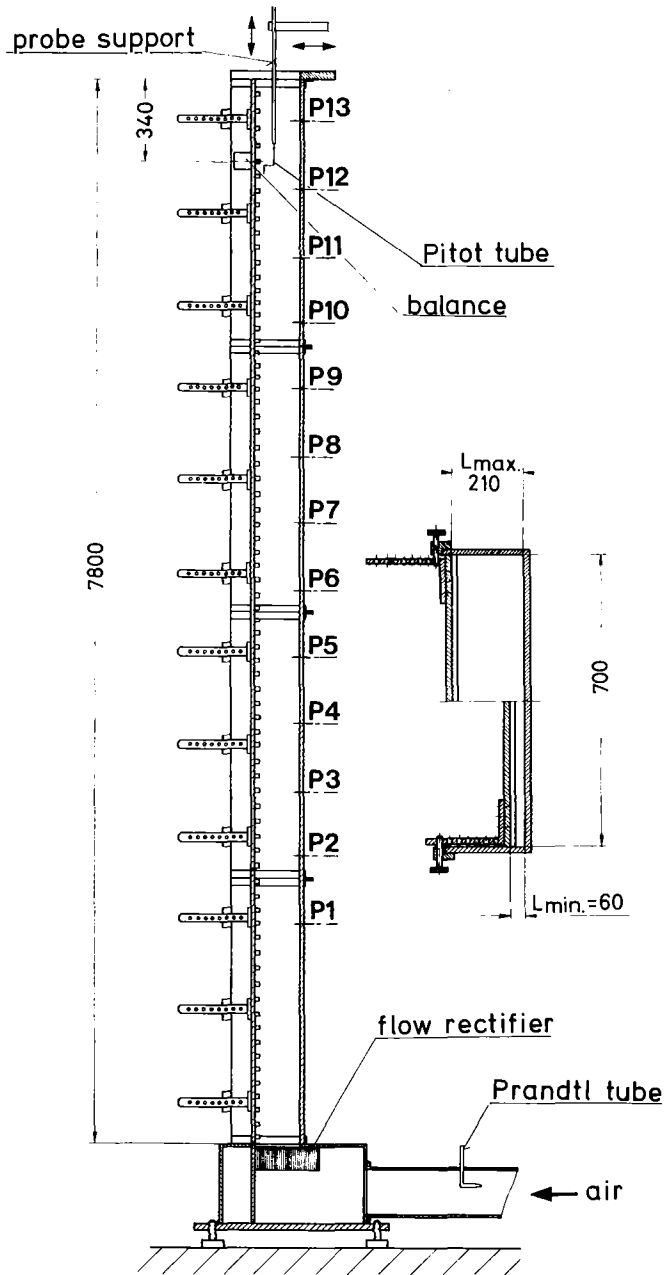


Fig. 1. The test section.

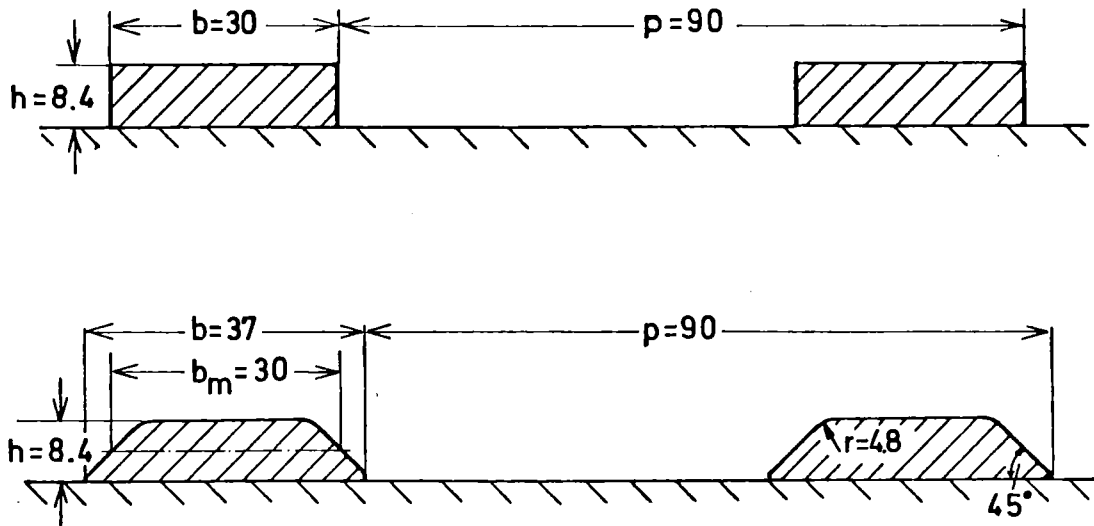


Fig. 2: Roughness geometry

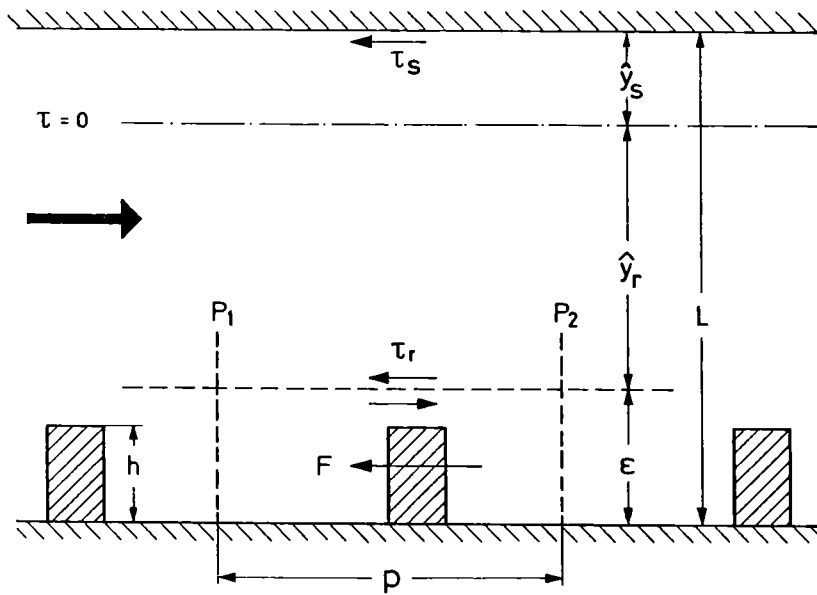


Fig. 3. Scheme of the flow cross section.

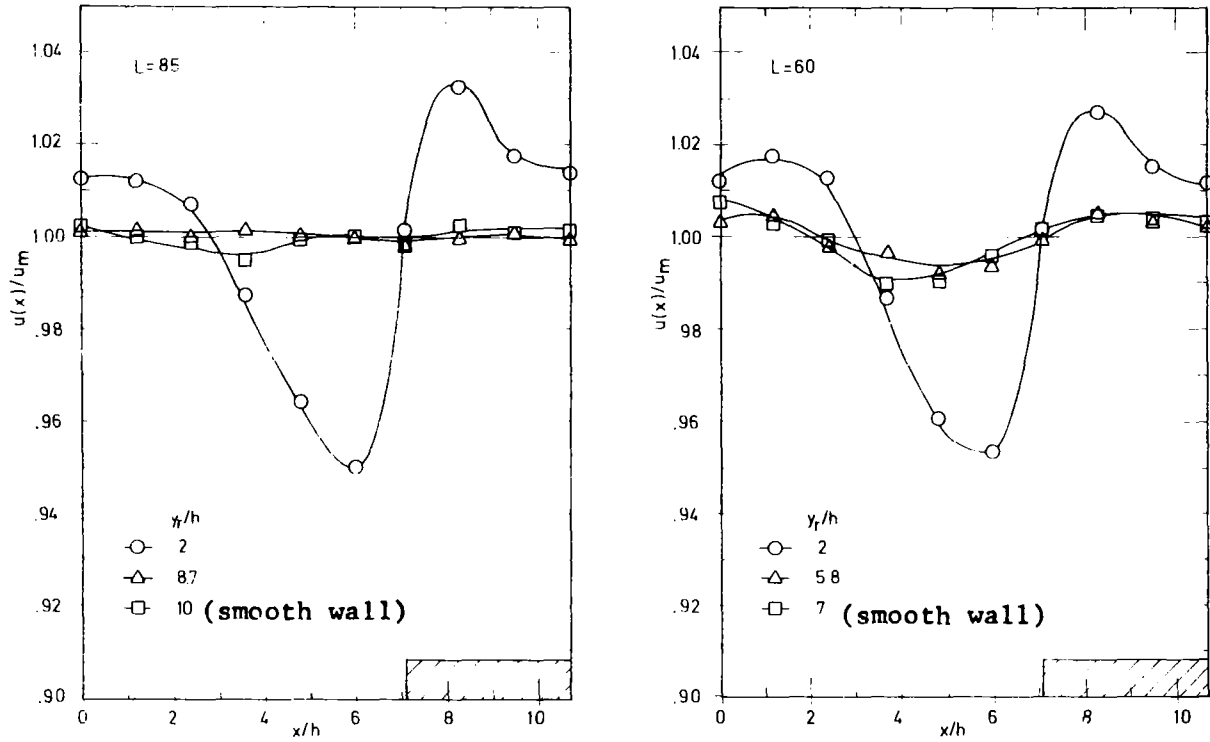


Fig. 4a: Axial velocity variation at the rectangular roughness

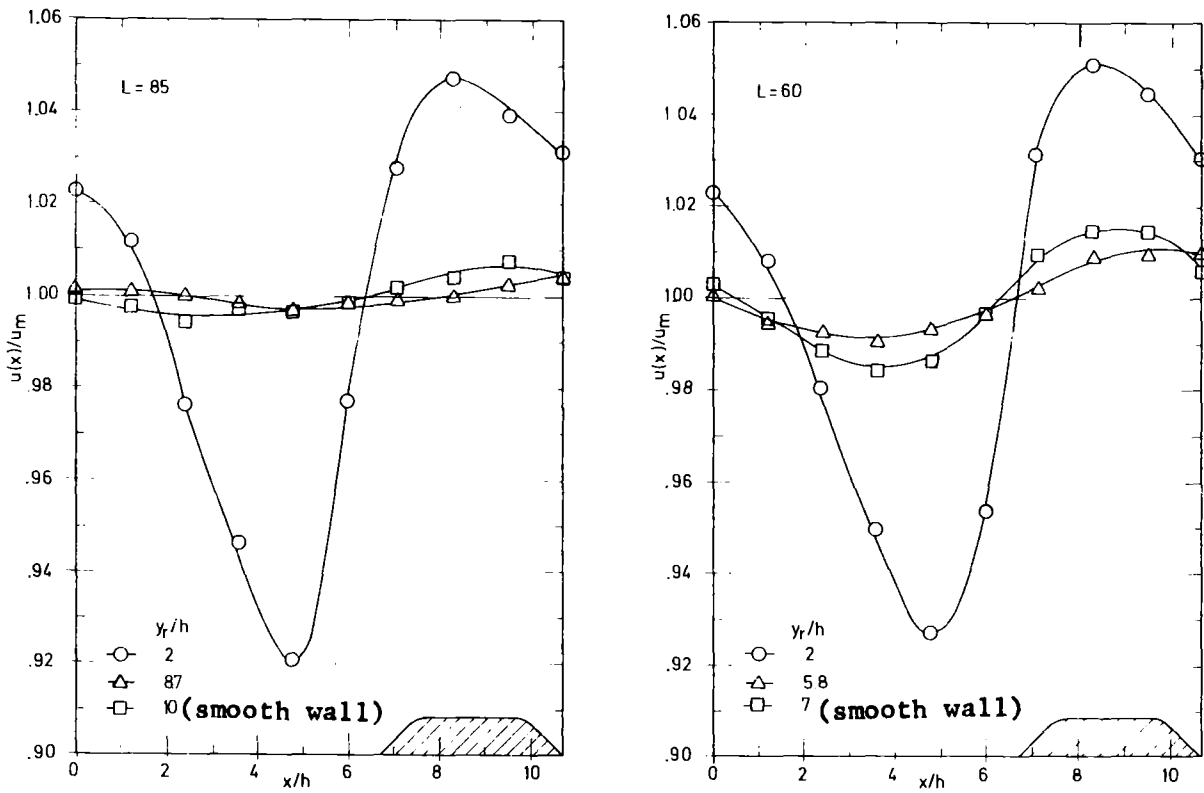


Fig. 4b: Axial velocity variation at the trapezoidal roughness

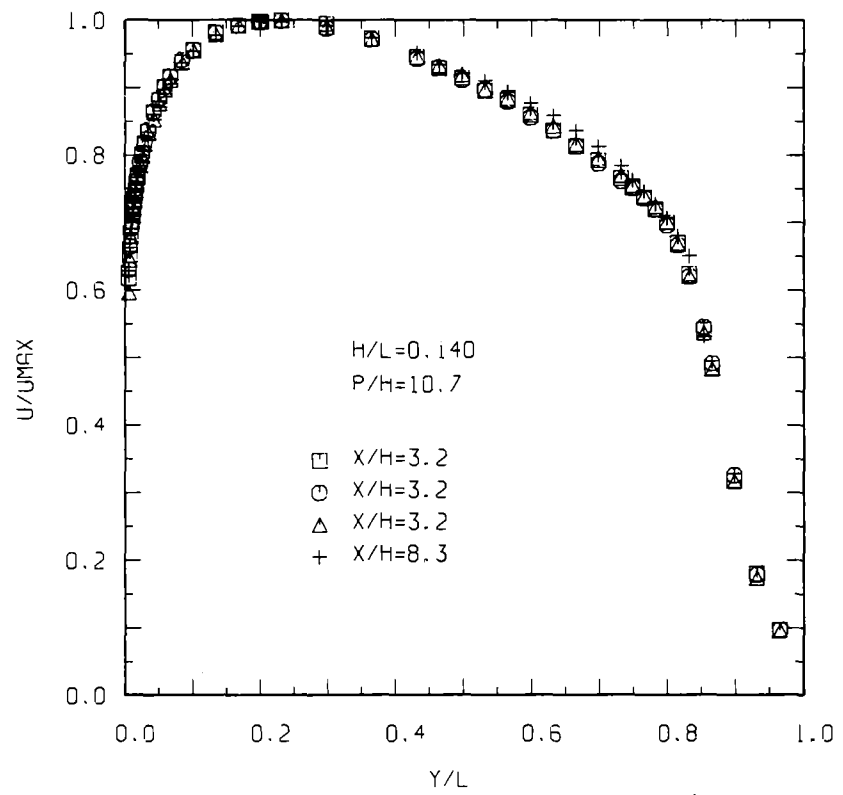
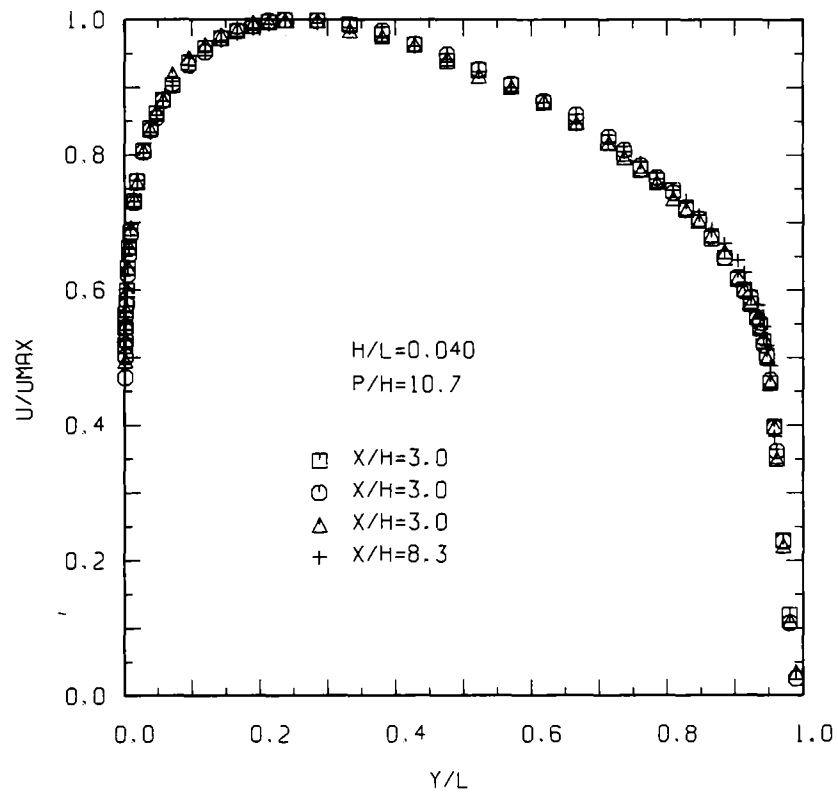


Fig. 5: Velocity distribution at maximum and minimum channel width with rectangular roughness

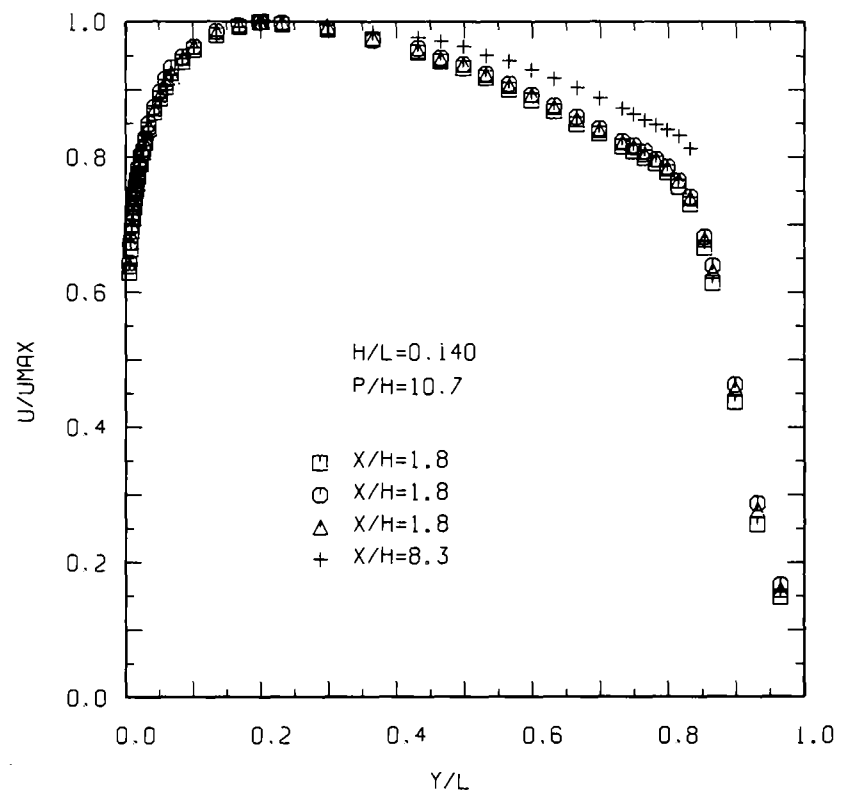
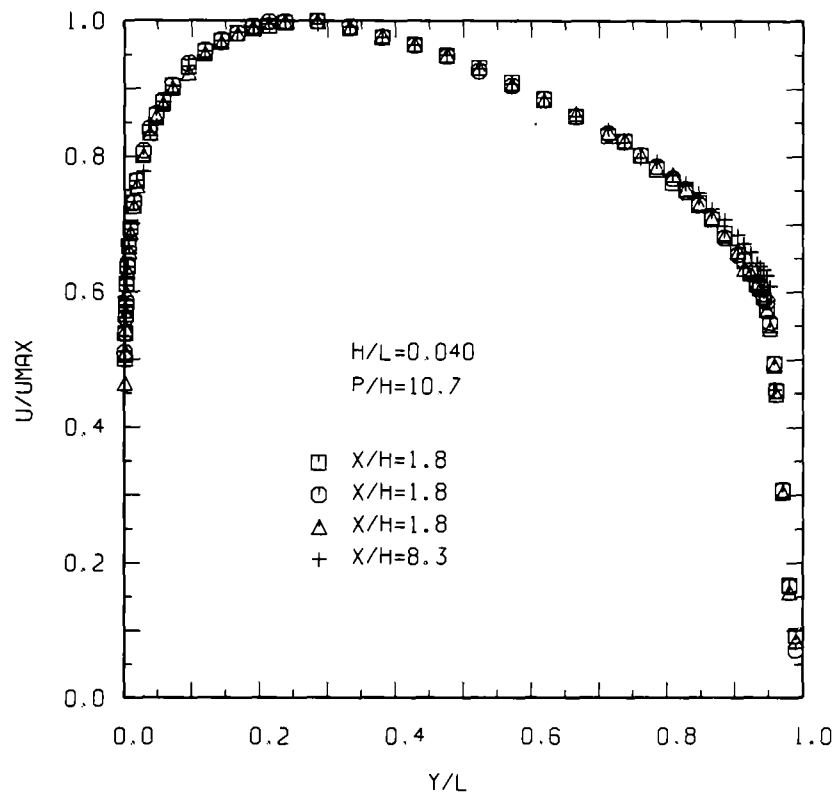


Fig. 6: Velocity distribution at maximum and minimum channel width with trapezoidal roughness

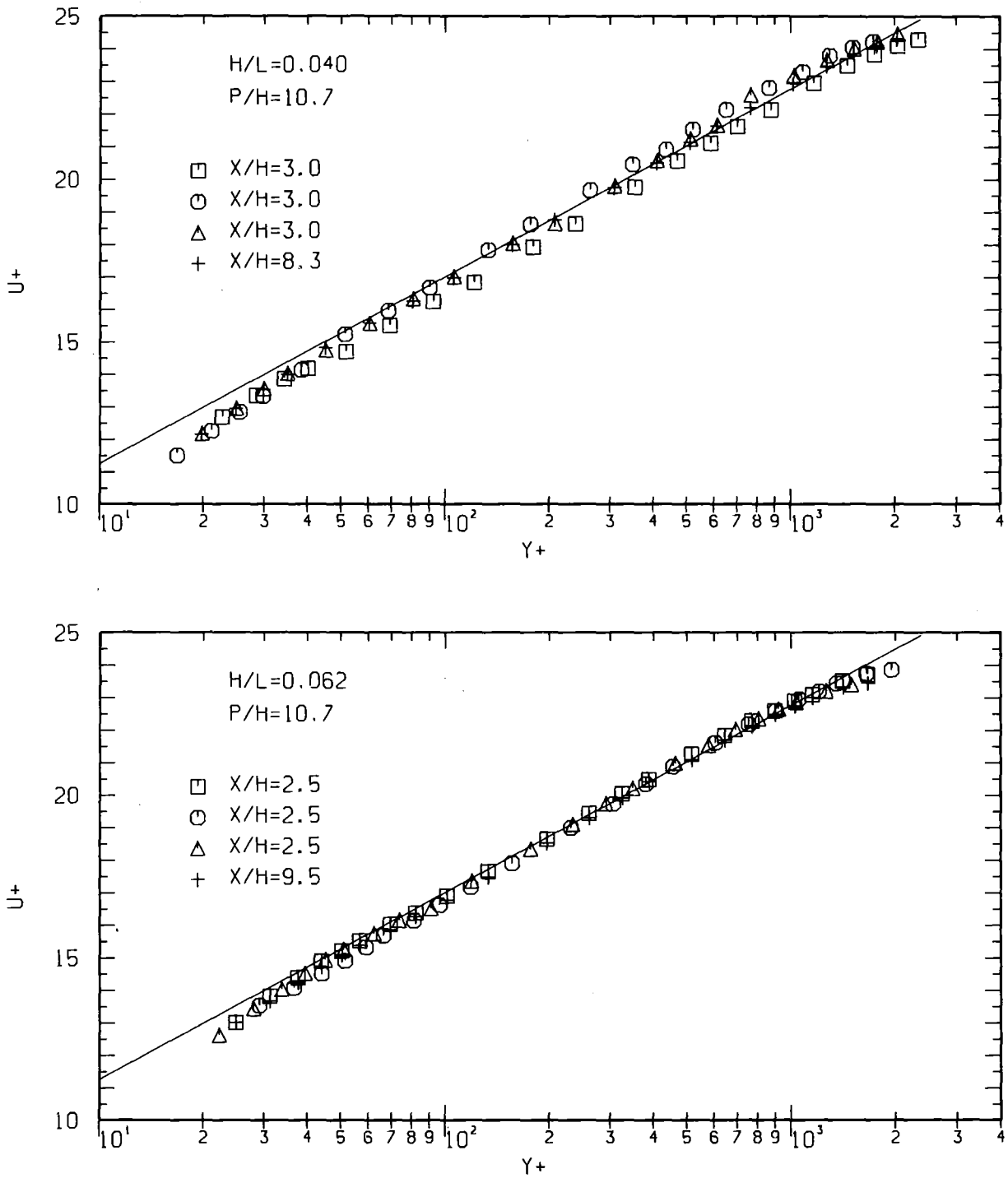


Fig. 7: Non-dimensional velocity profiles at the smooth wall with rectangular roughness at the opposite wall

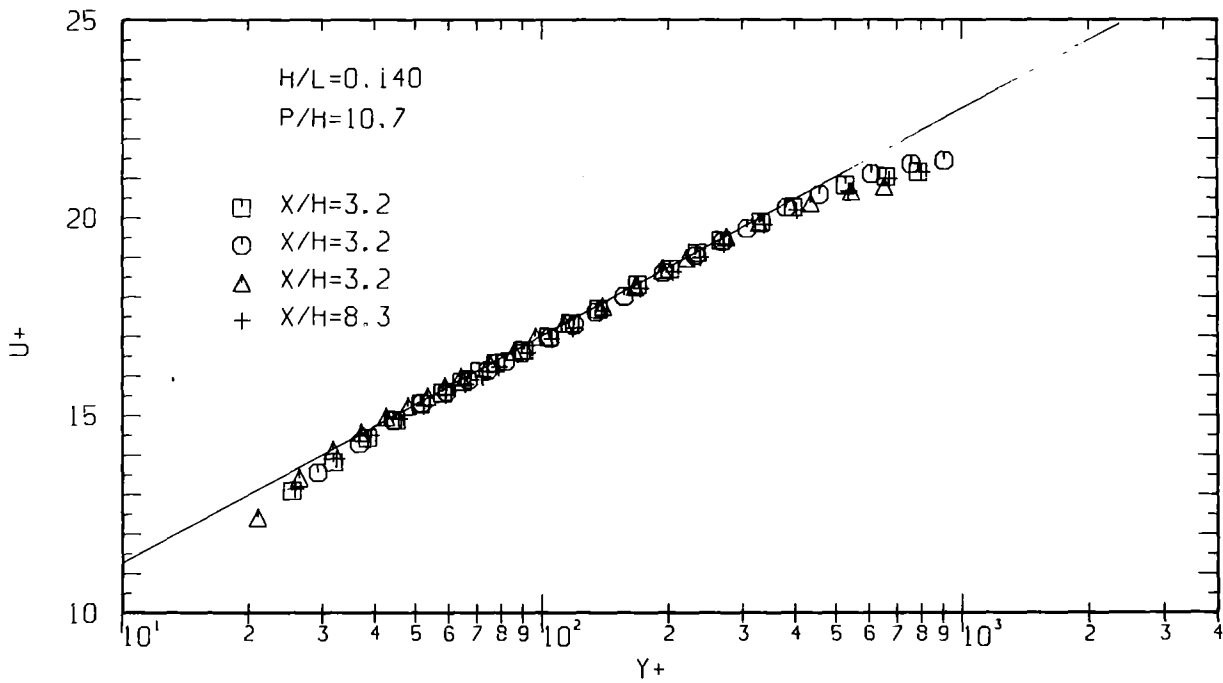
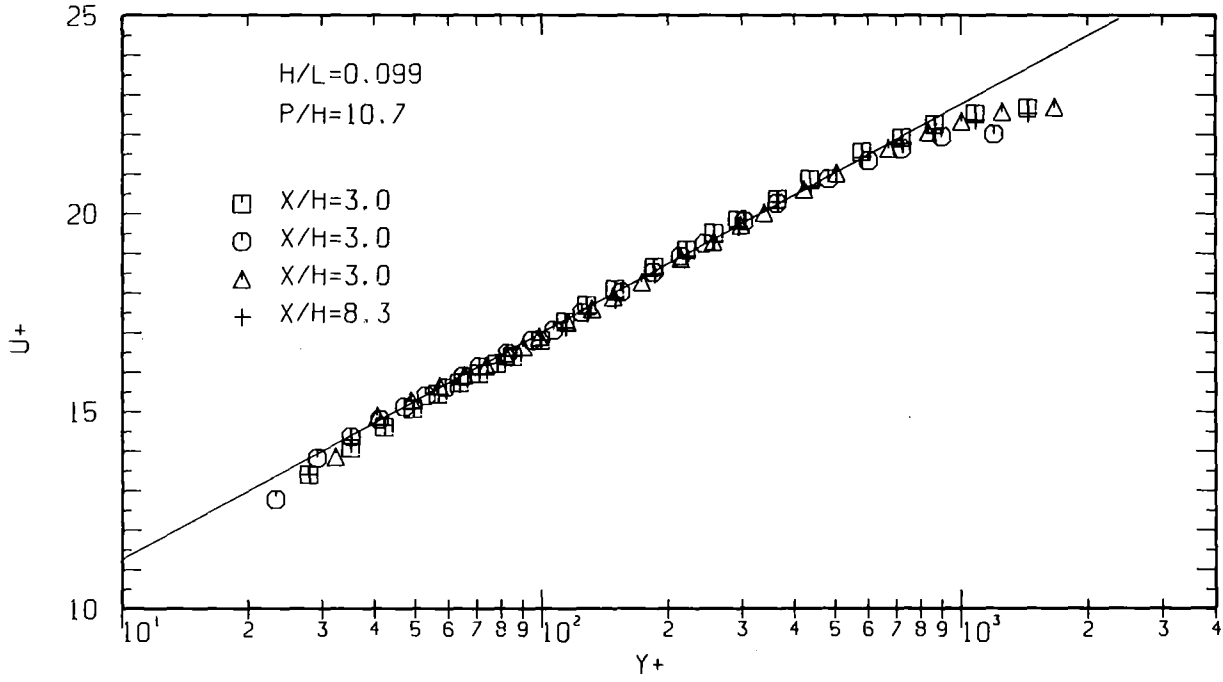


Fig. 8: Non-dimensional velocity profiles at the smooth wall with rectangular roughness at the opposite wall

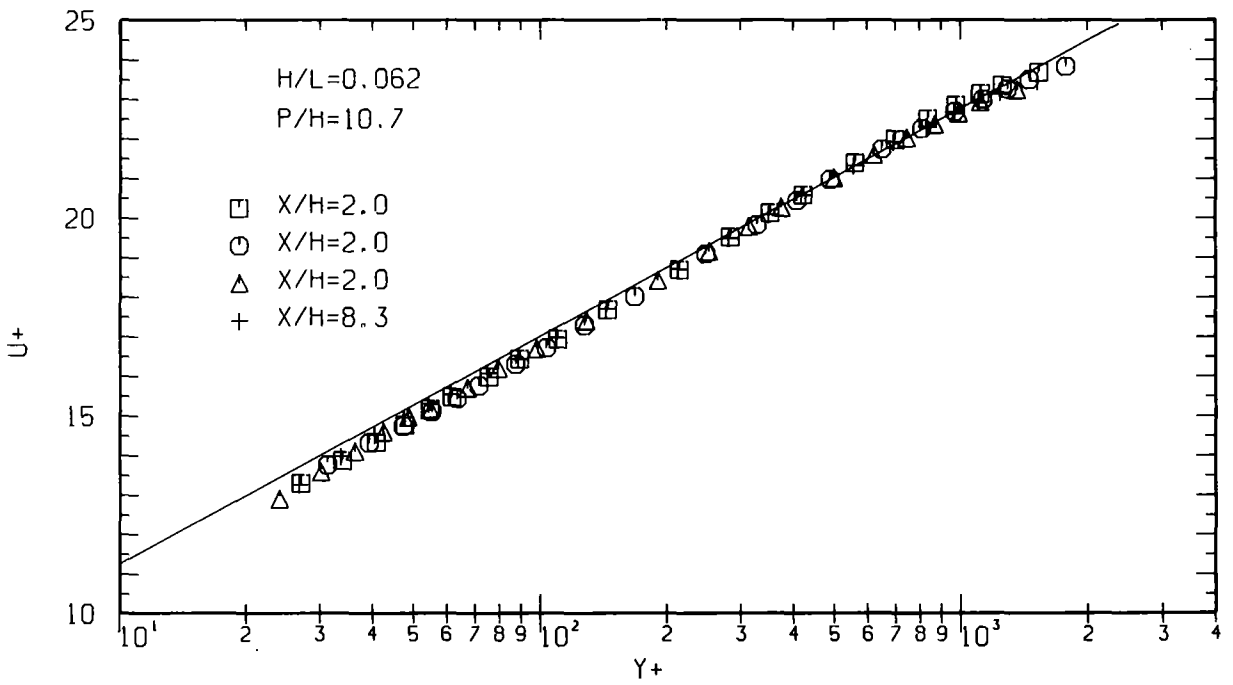
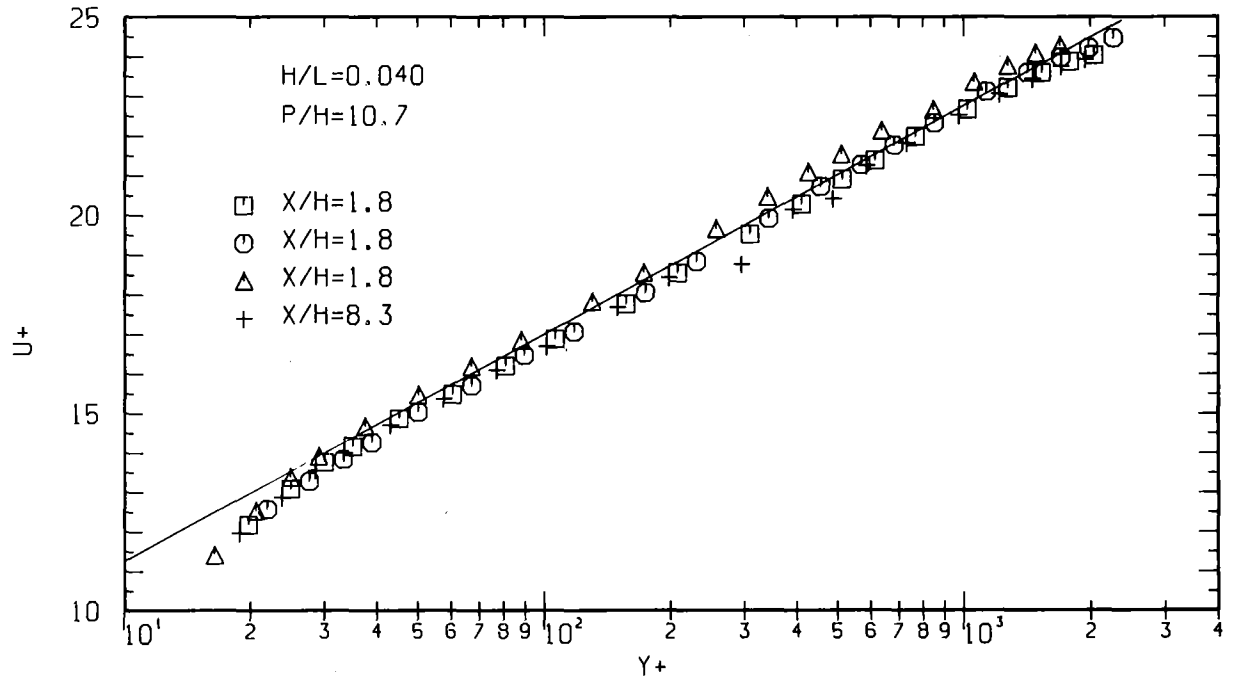


Fig.9: Non-dimensional velocity profiles at the smooth wall with trapezoidal roughness at the opposite wall

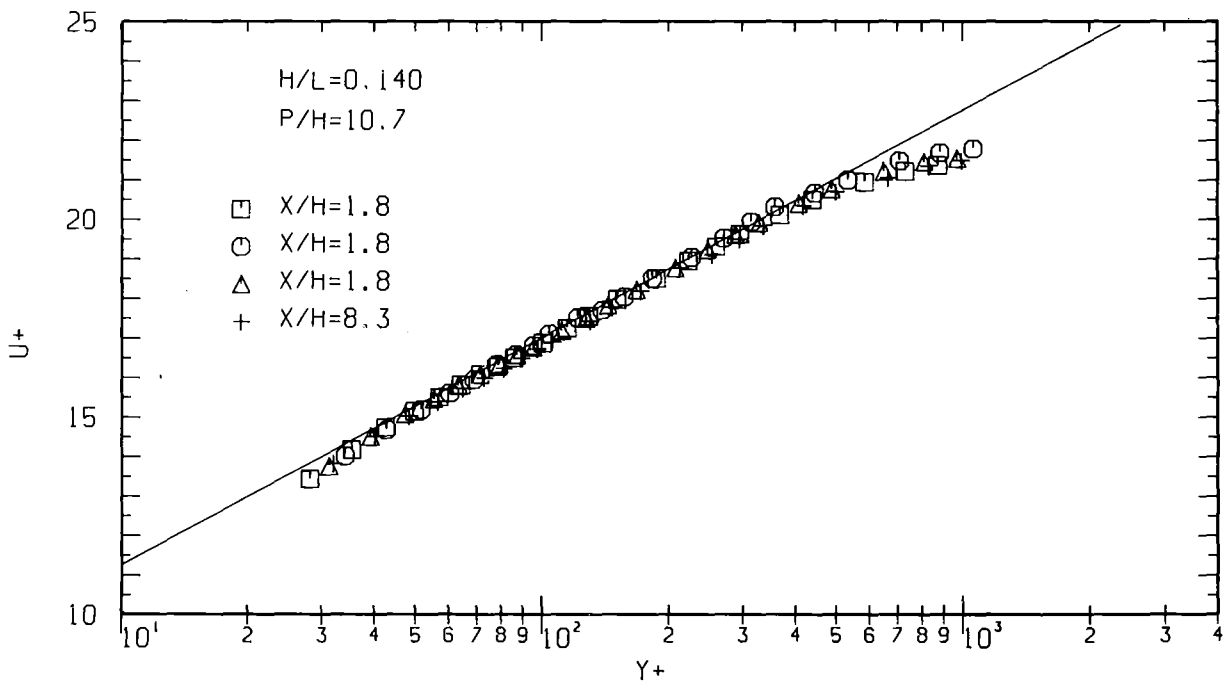
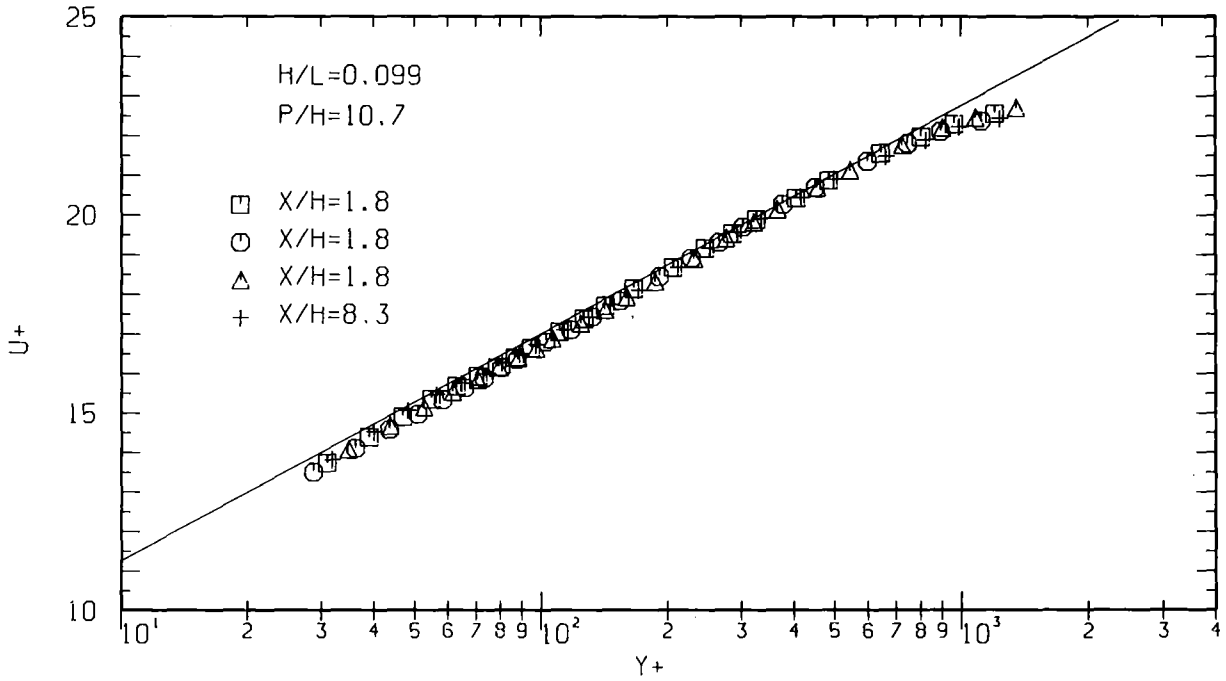


Fig.10: Non-dimensional velocity profiles at the smooth wall with trapezoidal roughness at the opposite wall

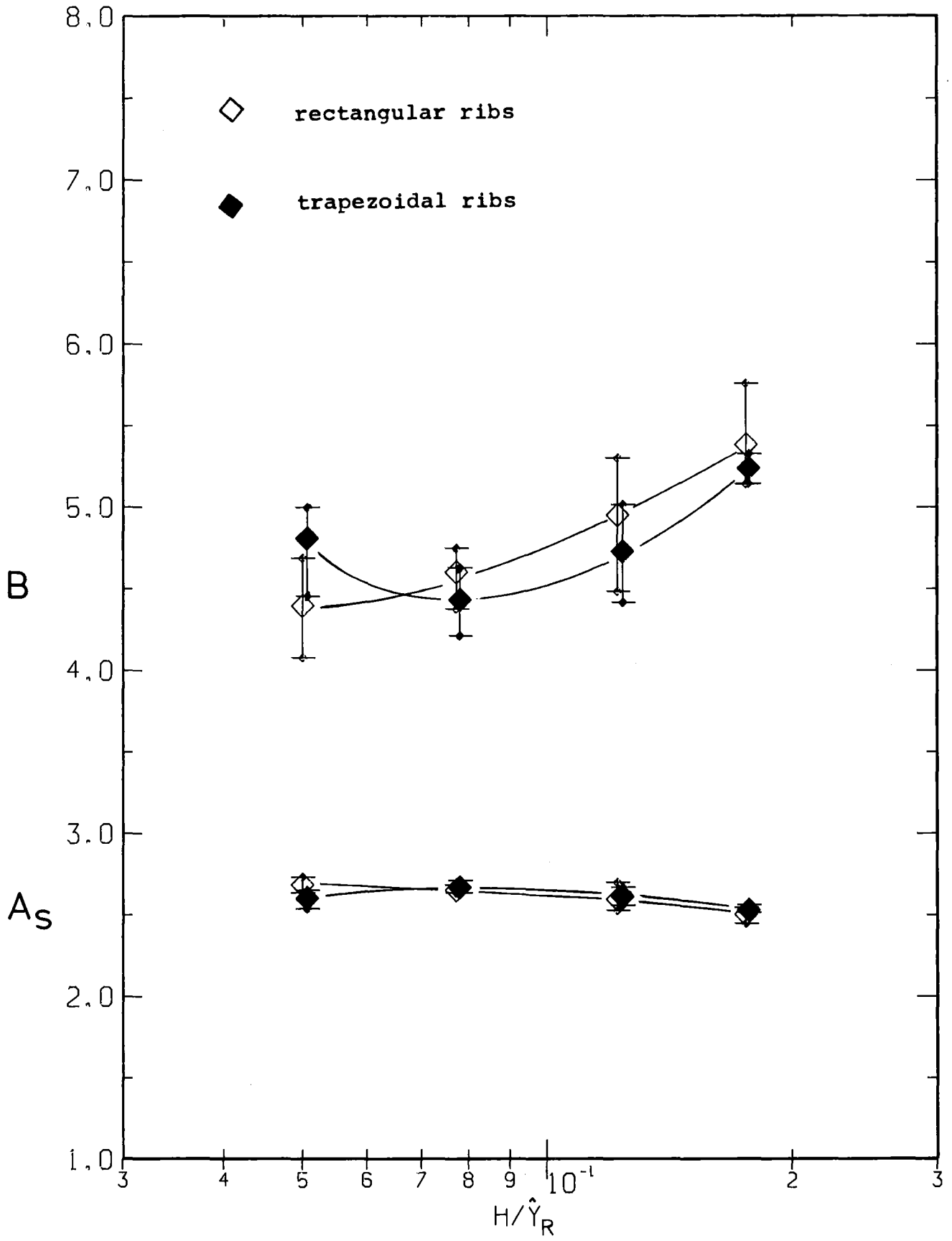


Fig.11: The parameters A_s and B of the smooth profile with roughness at opposite wall

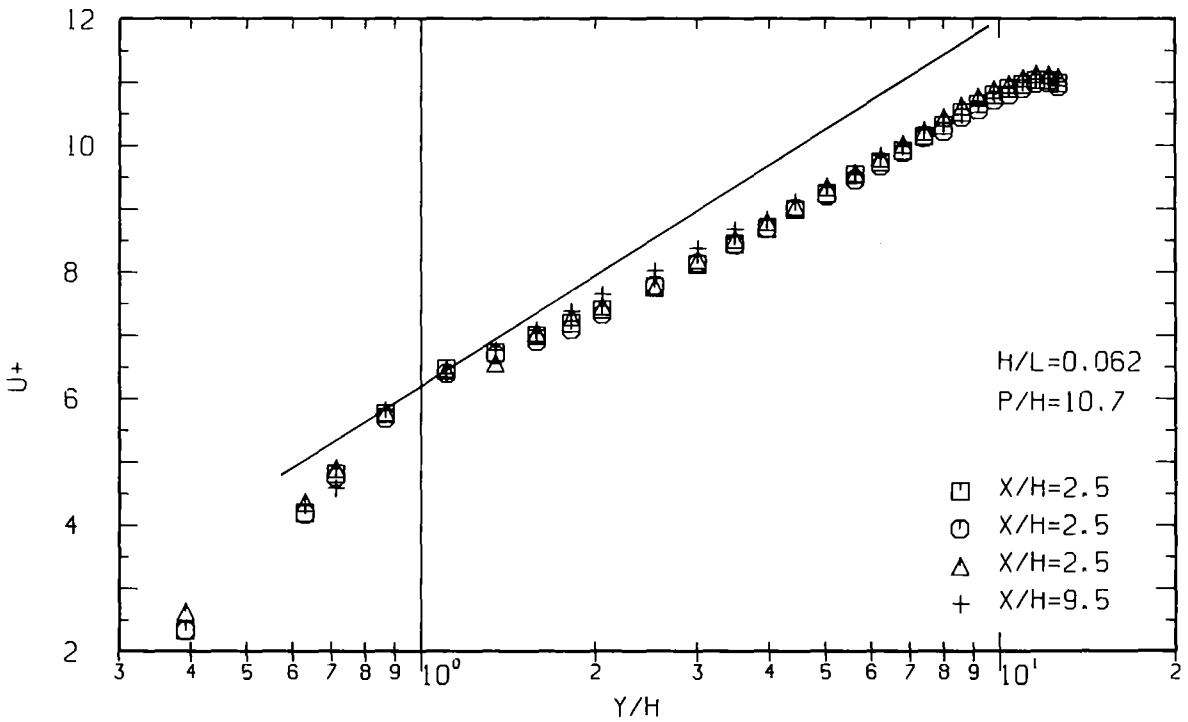
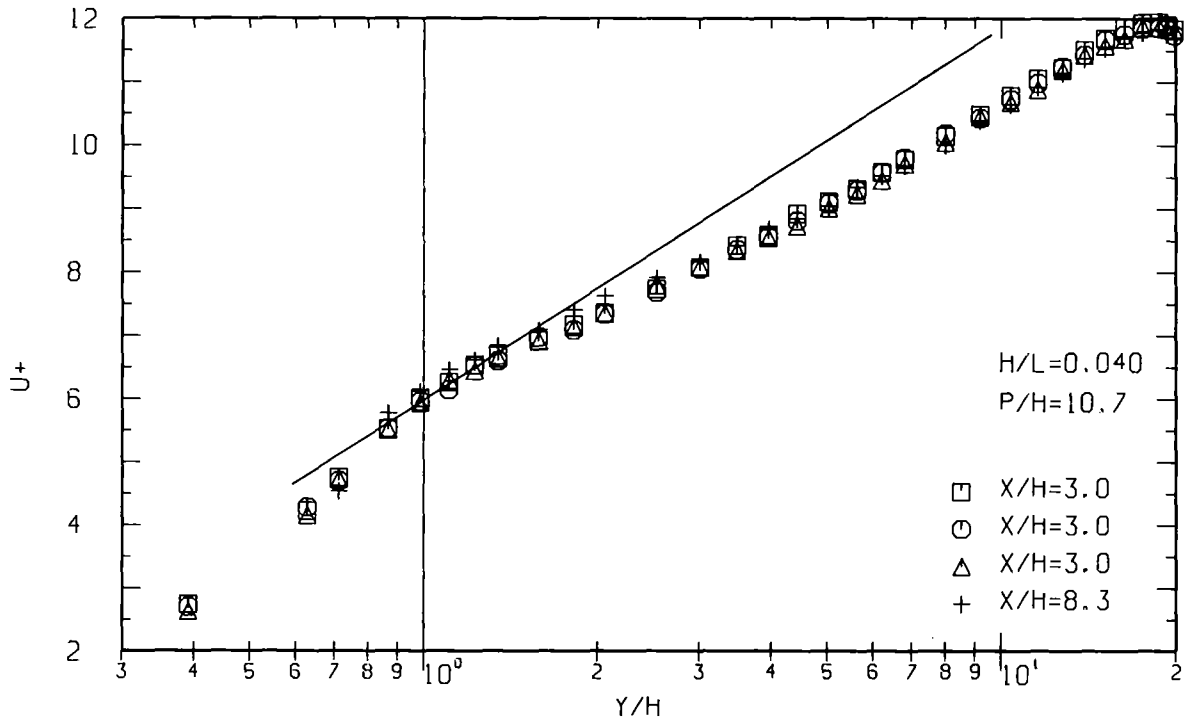


Fig.12: Non-dimensional velocity profiles at the rectangular roughness ($\epsilon=\epsilon_{vol}$)

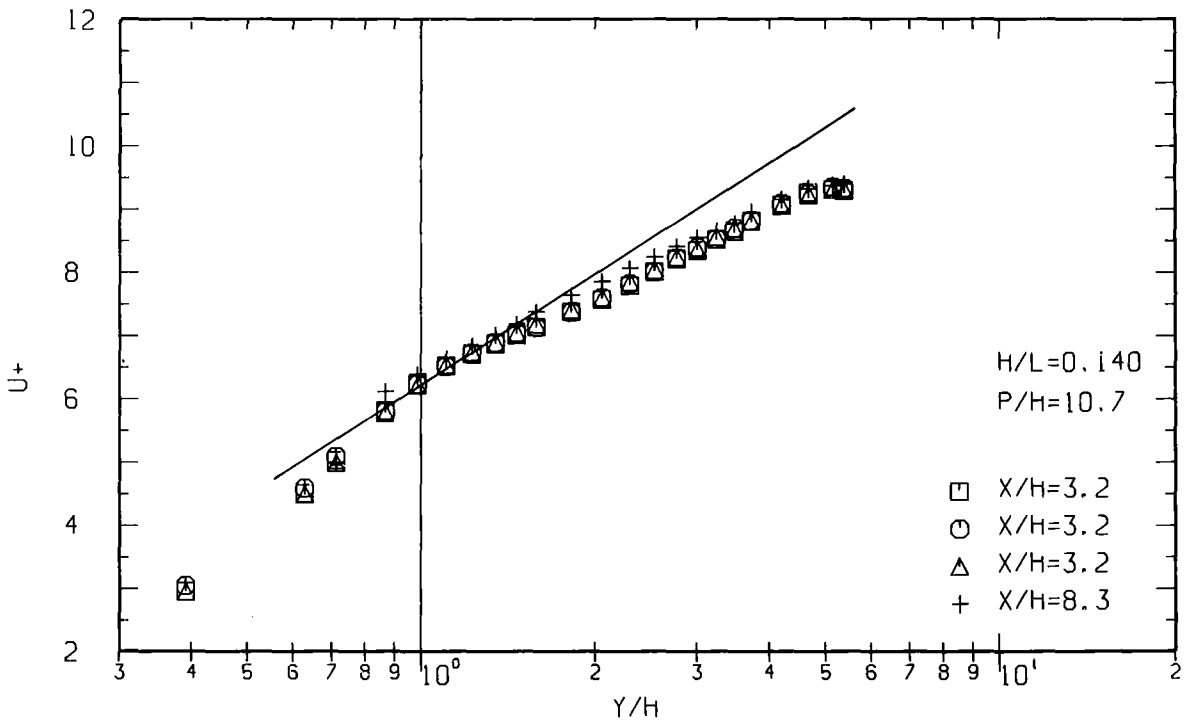
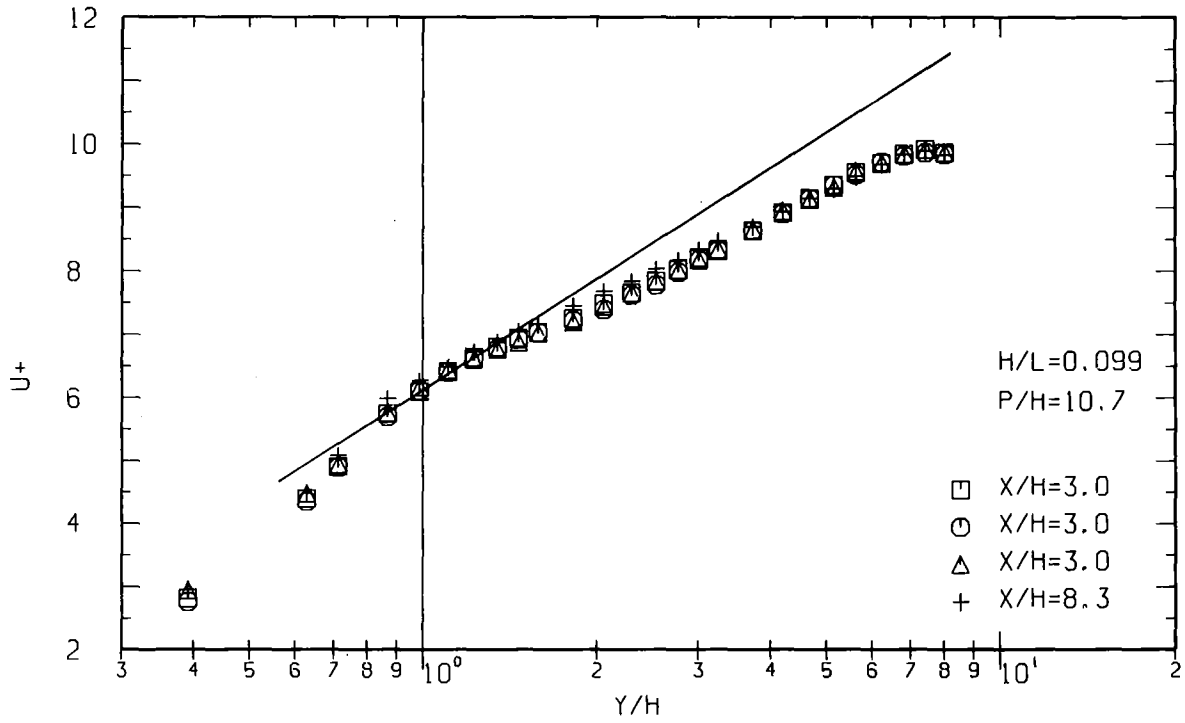


Fig.13: Non-dimensional velocity profiles at the rectangular roughness ($\epsilon=\epsilon_{vol}$)

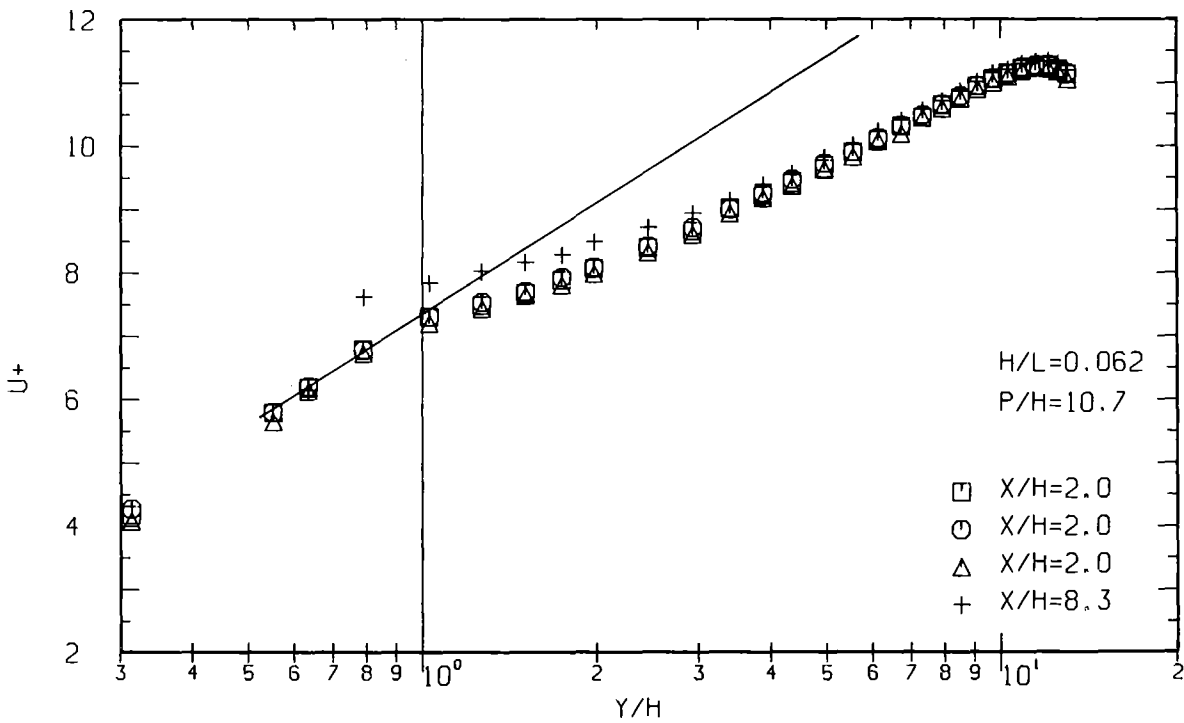
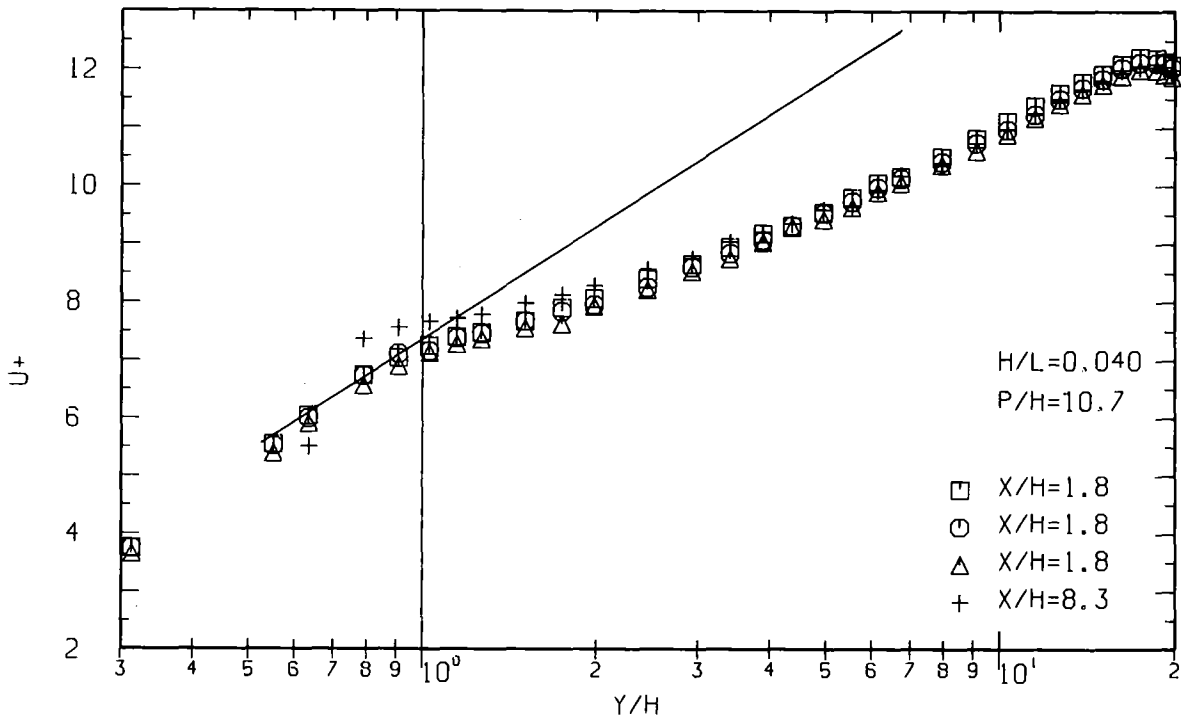


Fig.14: Non-dimensional velocity profiles at the trapezoidal roughness ($\epsilon=\epsilon_{vol}$)

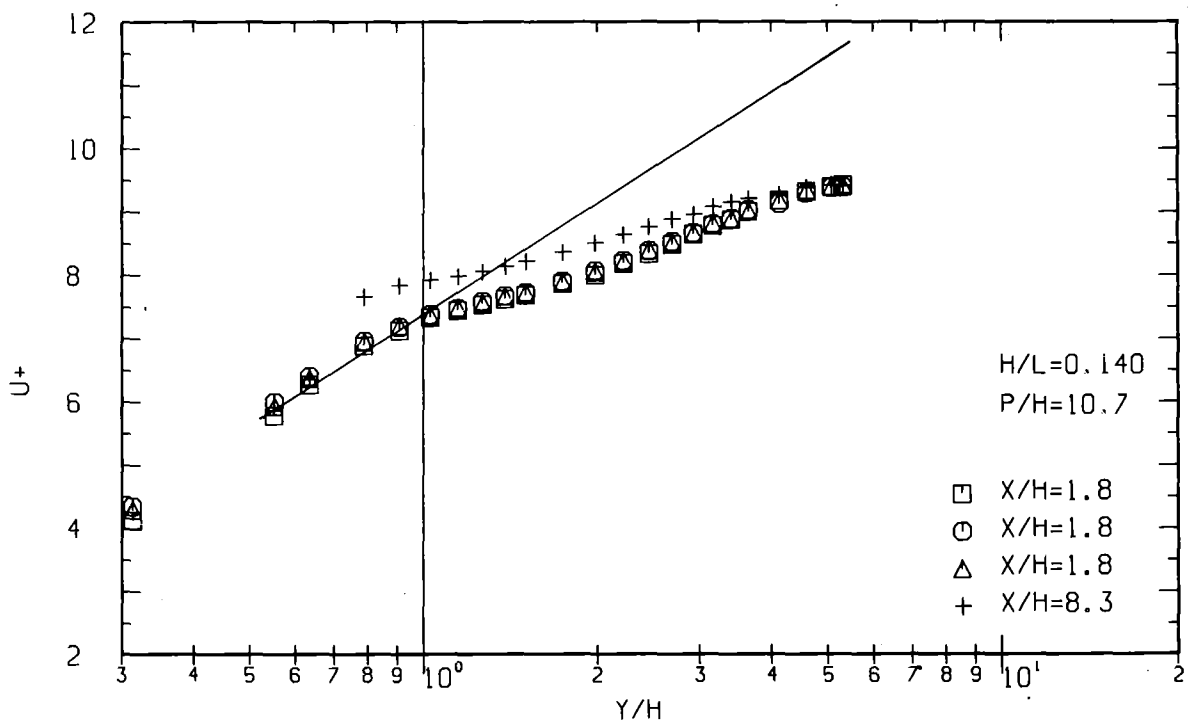
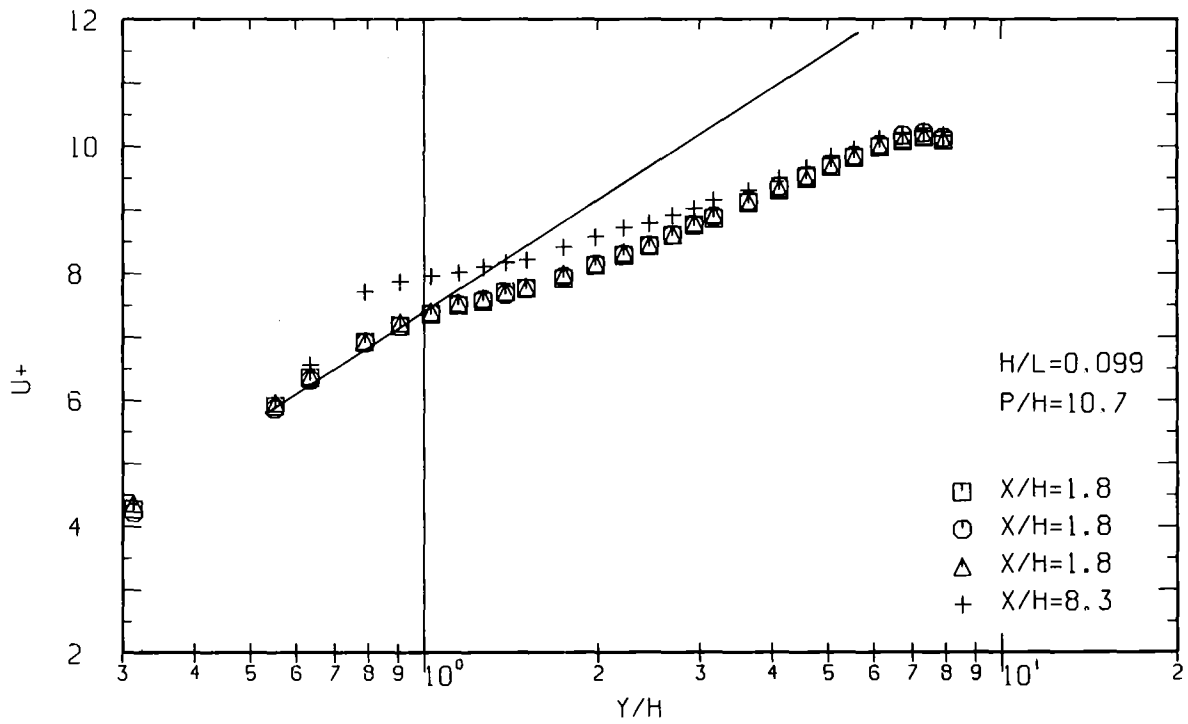


Fig.15: Non-dimensional velocity profiles at the trapezoidal roughness ($\epsilon=\epsilon_{vol}$)

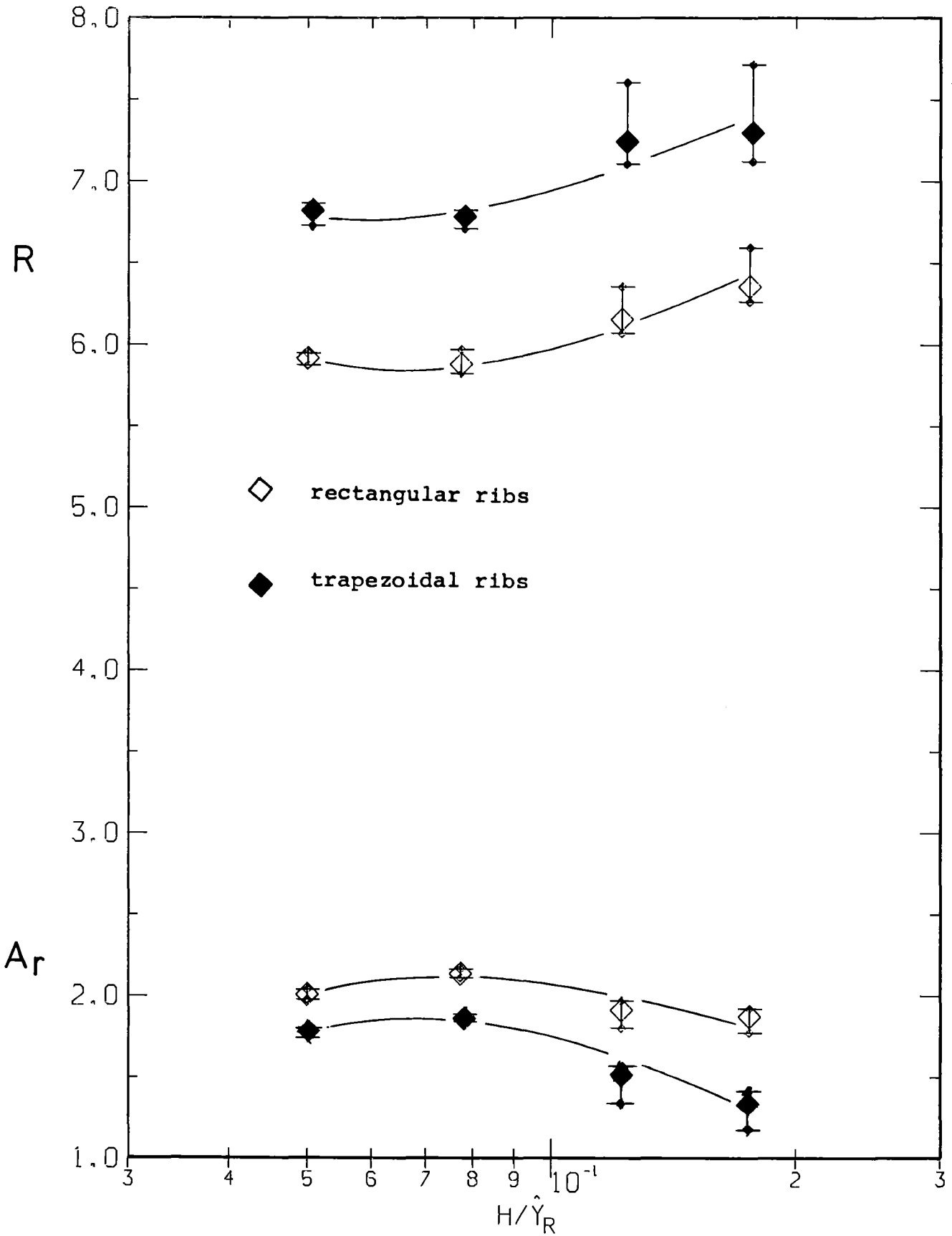


Fig.16: The Parameters A_r and R of the rough profiles with volumetrical definition of the origin of the velocity profile ($\epsilon = \epsilon_{vol}$)

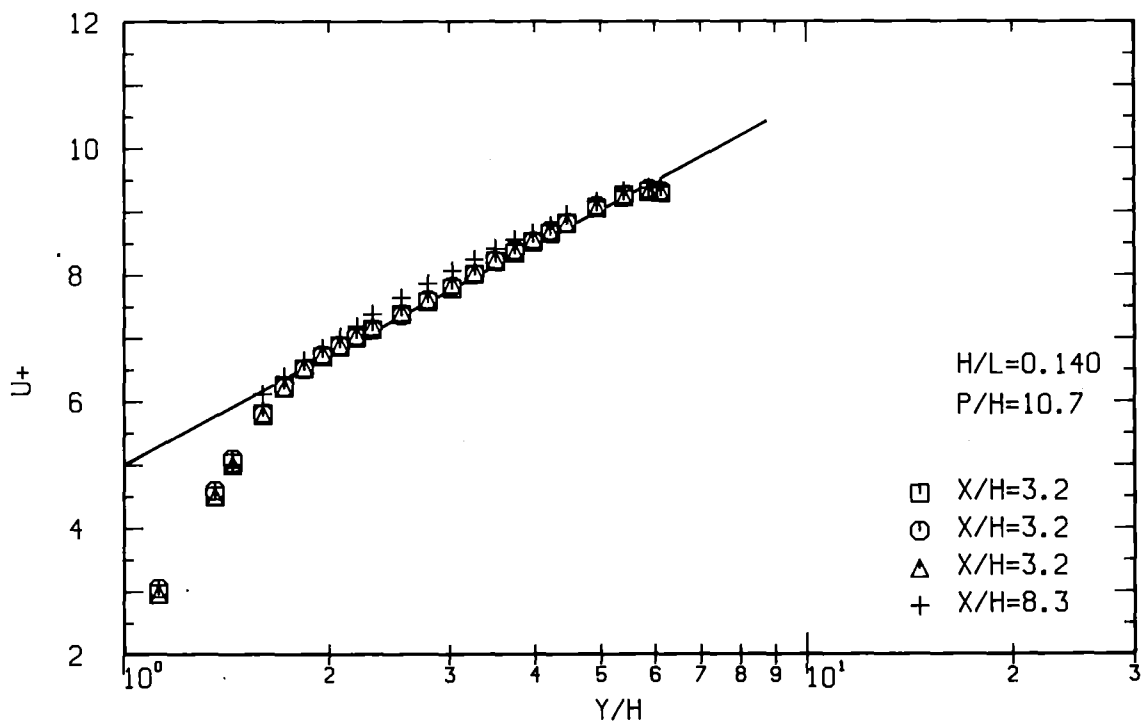
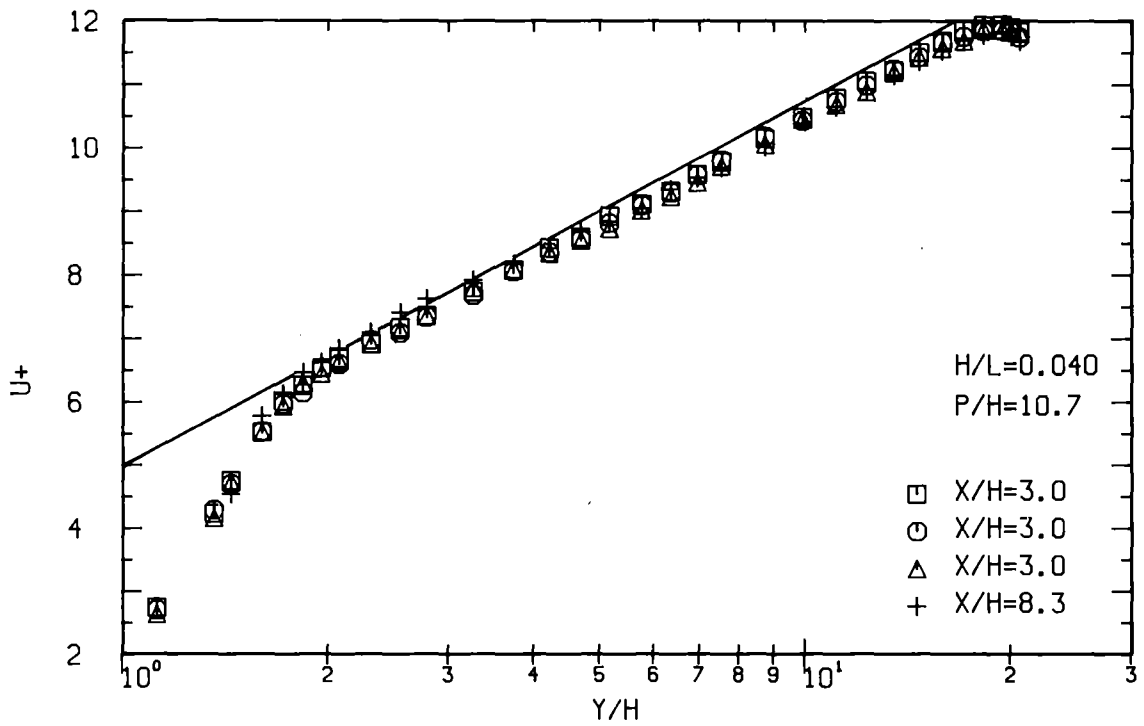


Fig.17: Non-dimensional velocity profiles at the rectangular roughness with negative origin of the profil ($\epsilon/h=-0.4$)

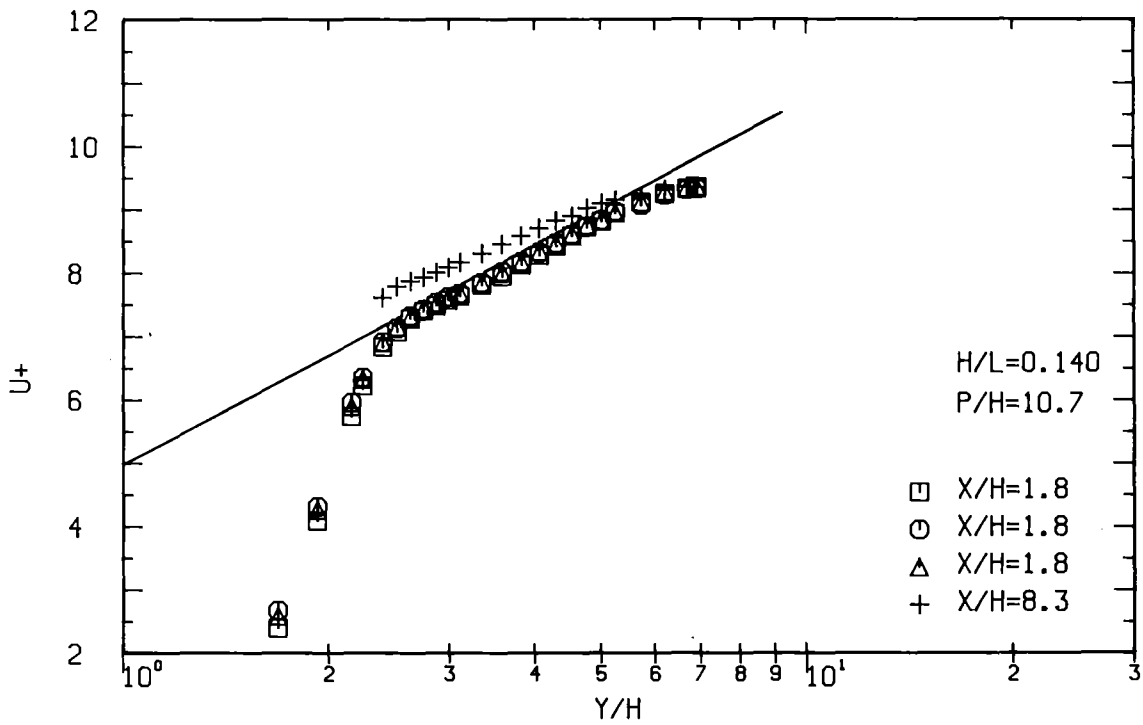
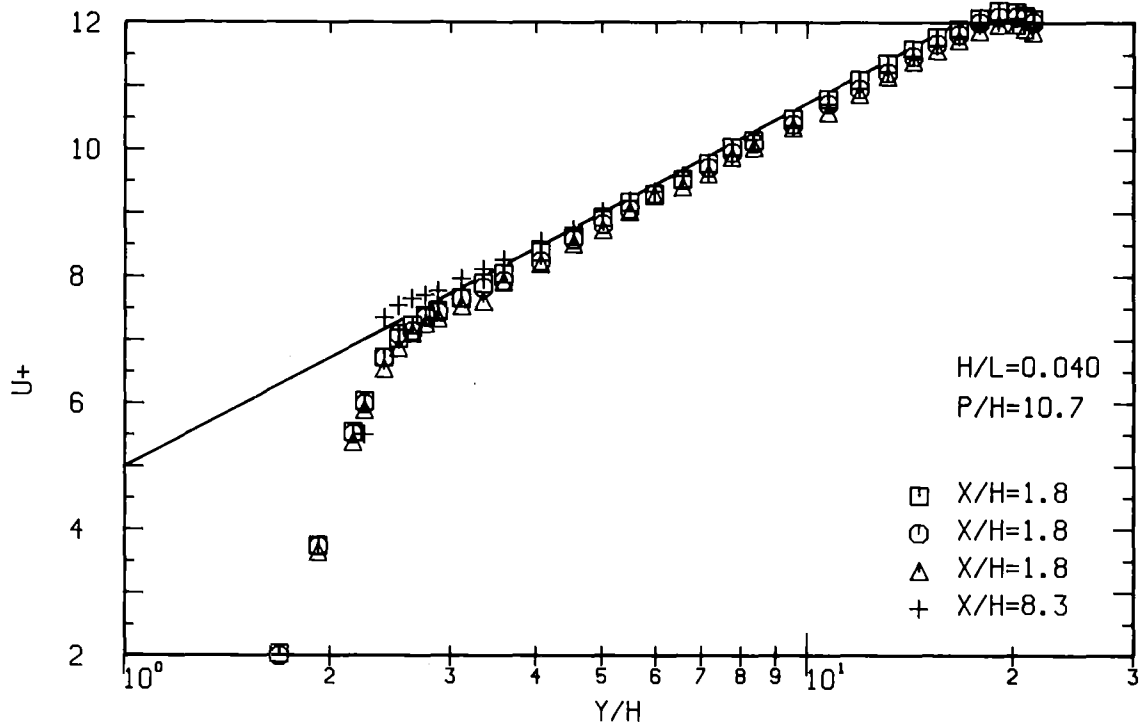


Fig.18: Non-dimensional velocity profiles at the trapezoidal roughness with negative origin of the profile ($\epsilon/h=-1.2$)

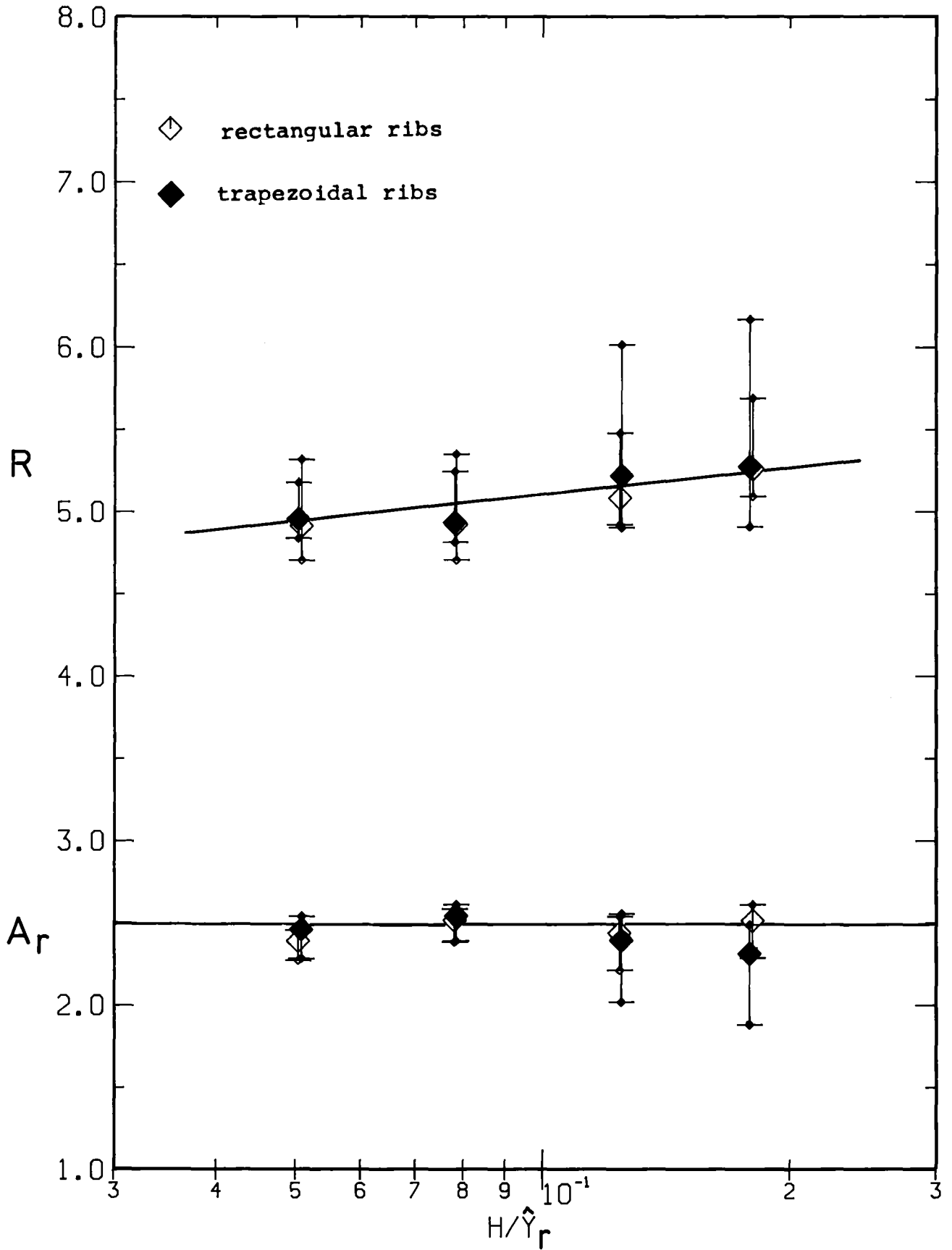


Fig.19: The parameters A_r and R of the rough profiles with negative definition of profile origin ($\epsilon_{rec}=-0.4h$; $\epsilon_{trap}=-1.2h$)

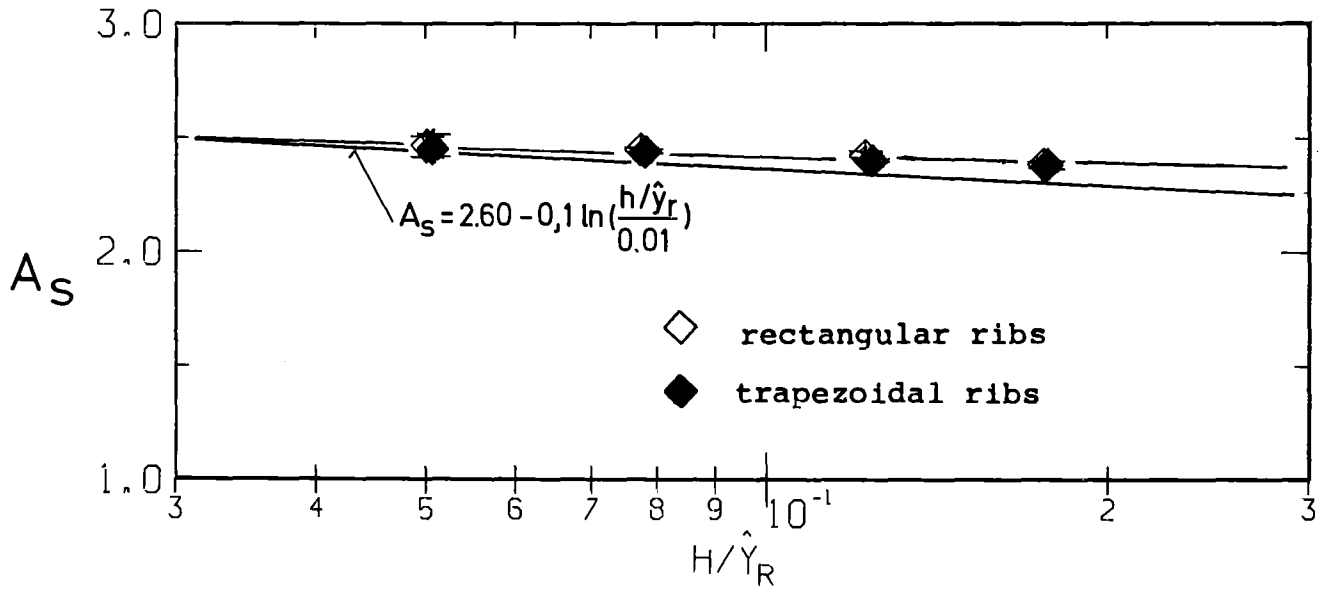


Fig.20a: The parameter A_S determined by equation (14) with $B=5.5$ as function of h/\hat{y}_R .

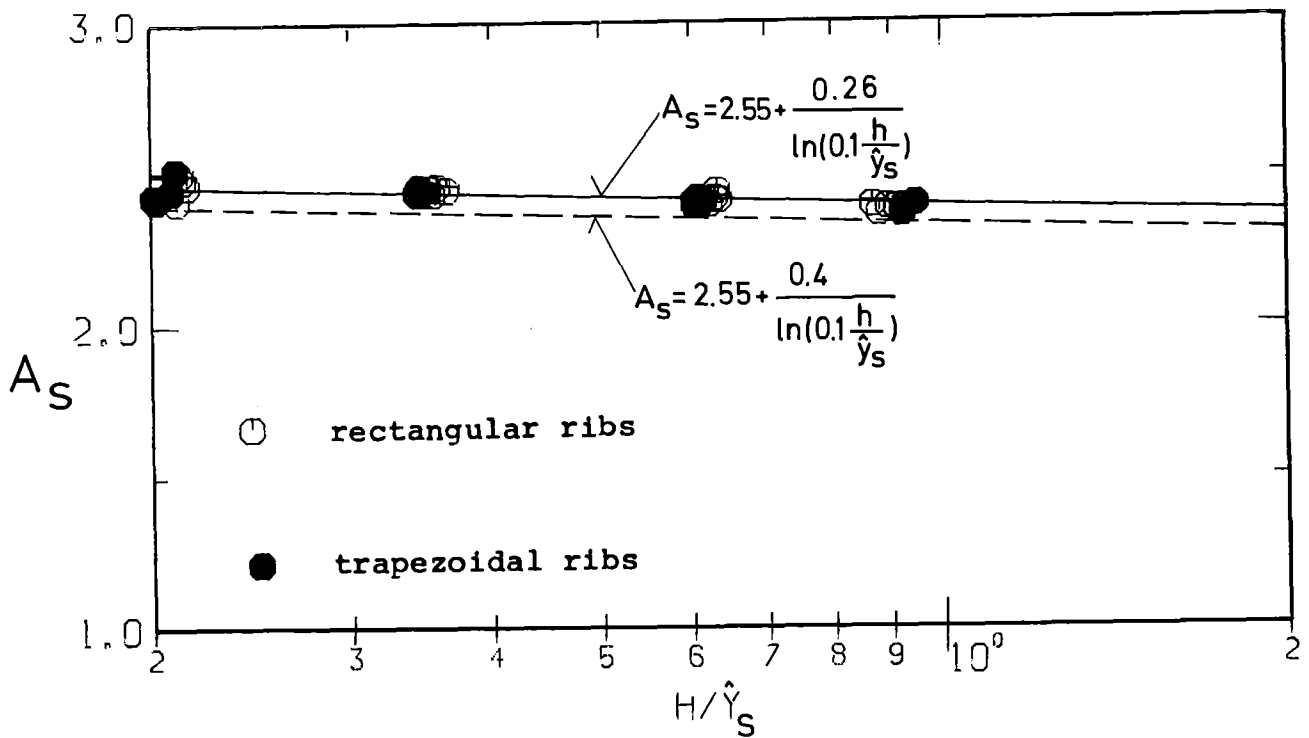


Fig.20b: The parameter A_S determined by equation (14) with $B=5.5$ as function of h/\hat{y}_S .

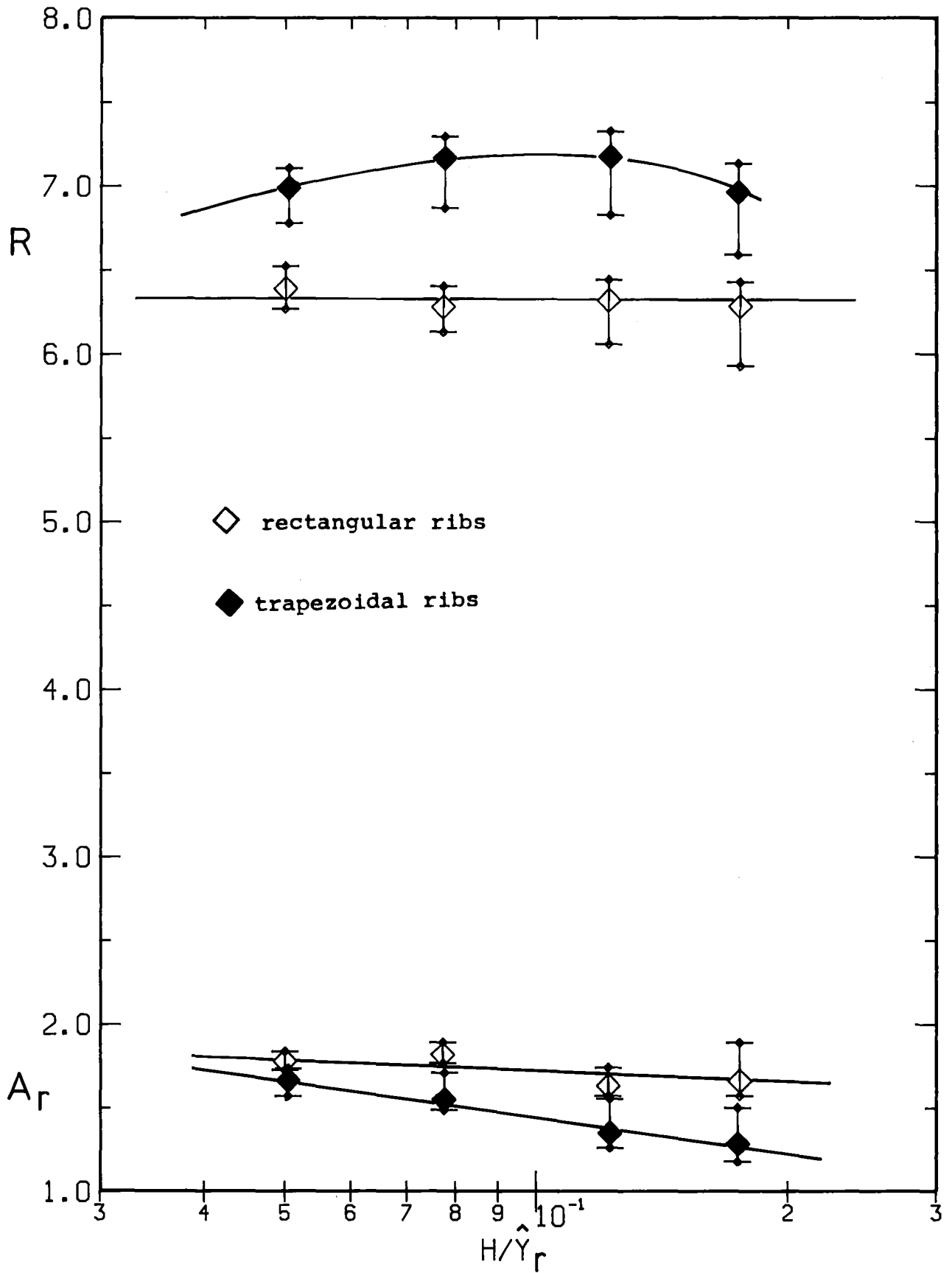


Fig.21: The parameters A_r and R determined by equations (14), (15) and (16) with $B=5.5$ and $\epsilon=\epsilon_{vol}$.

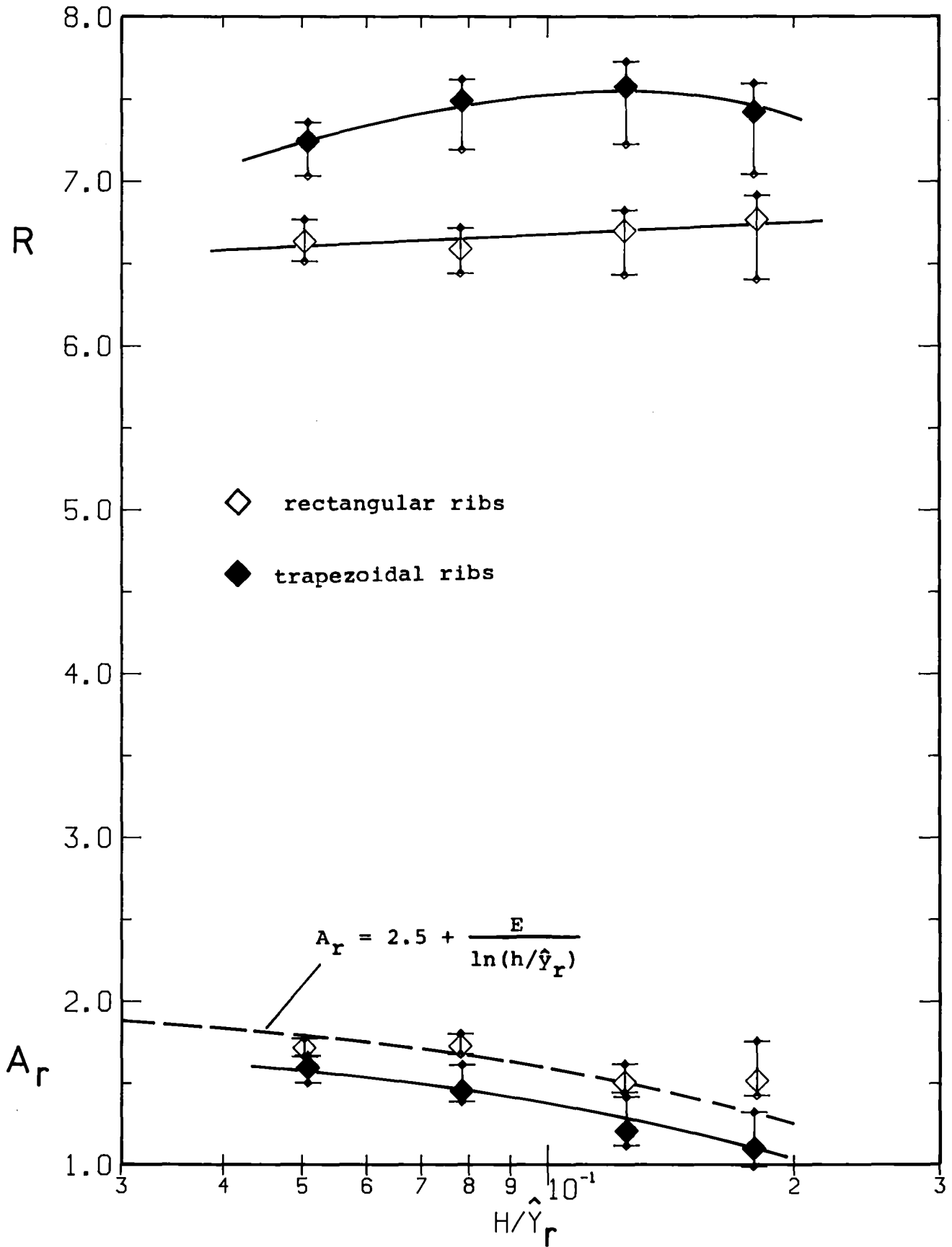


Fig.22: The parameters A_r and R determined by equations (14), (15) and (16) with $B=5.5$ and $\epsilon=\epsilon_{vol}^*$

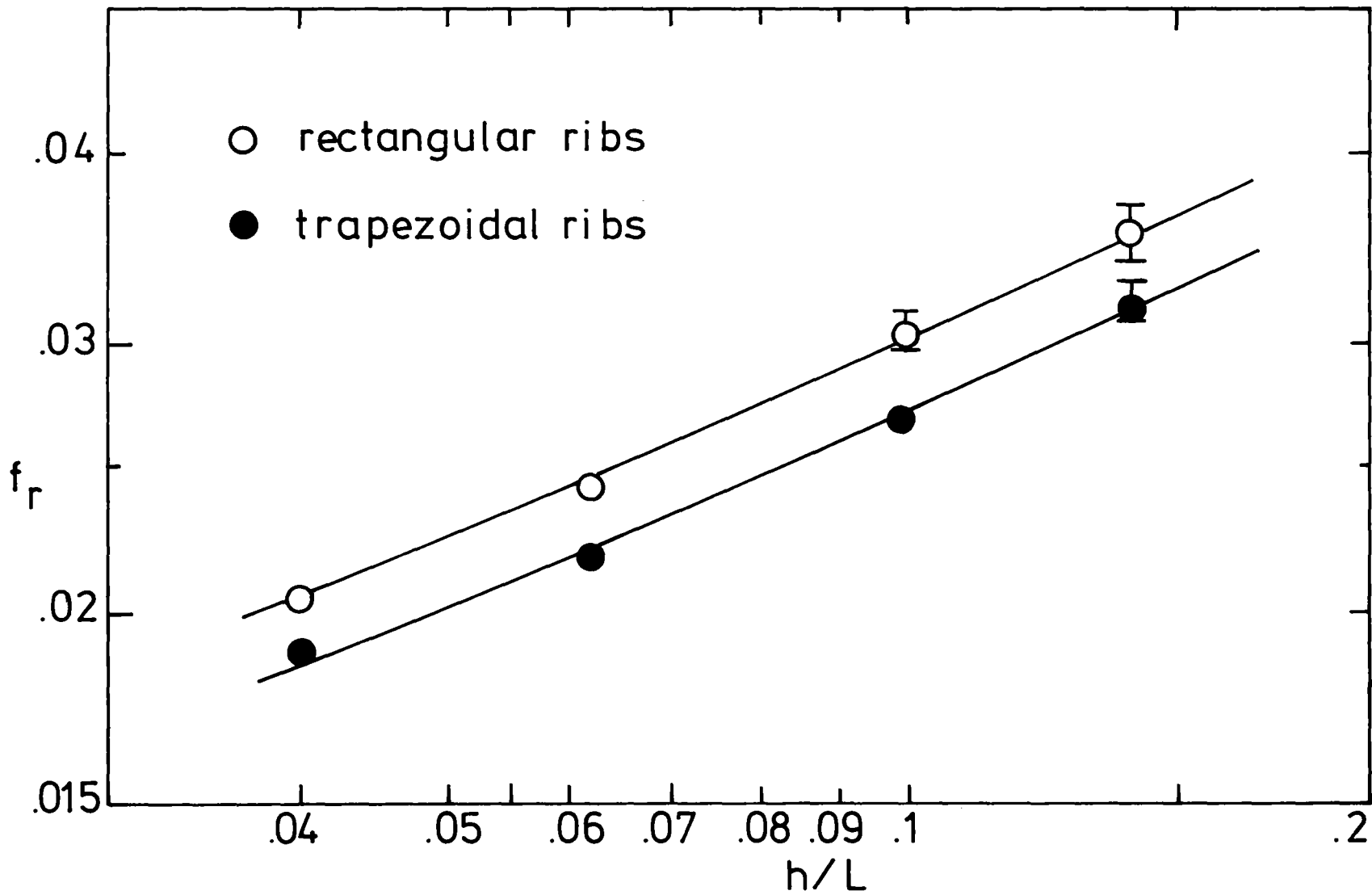


Fig. 23: The friction factor f_r of the rough zone as function of the relative roughness height ($\epsilon = \epsilon_{vol}$)

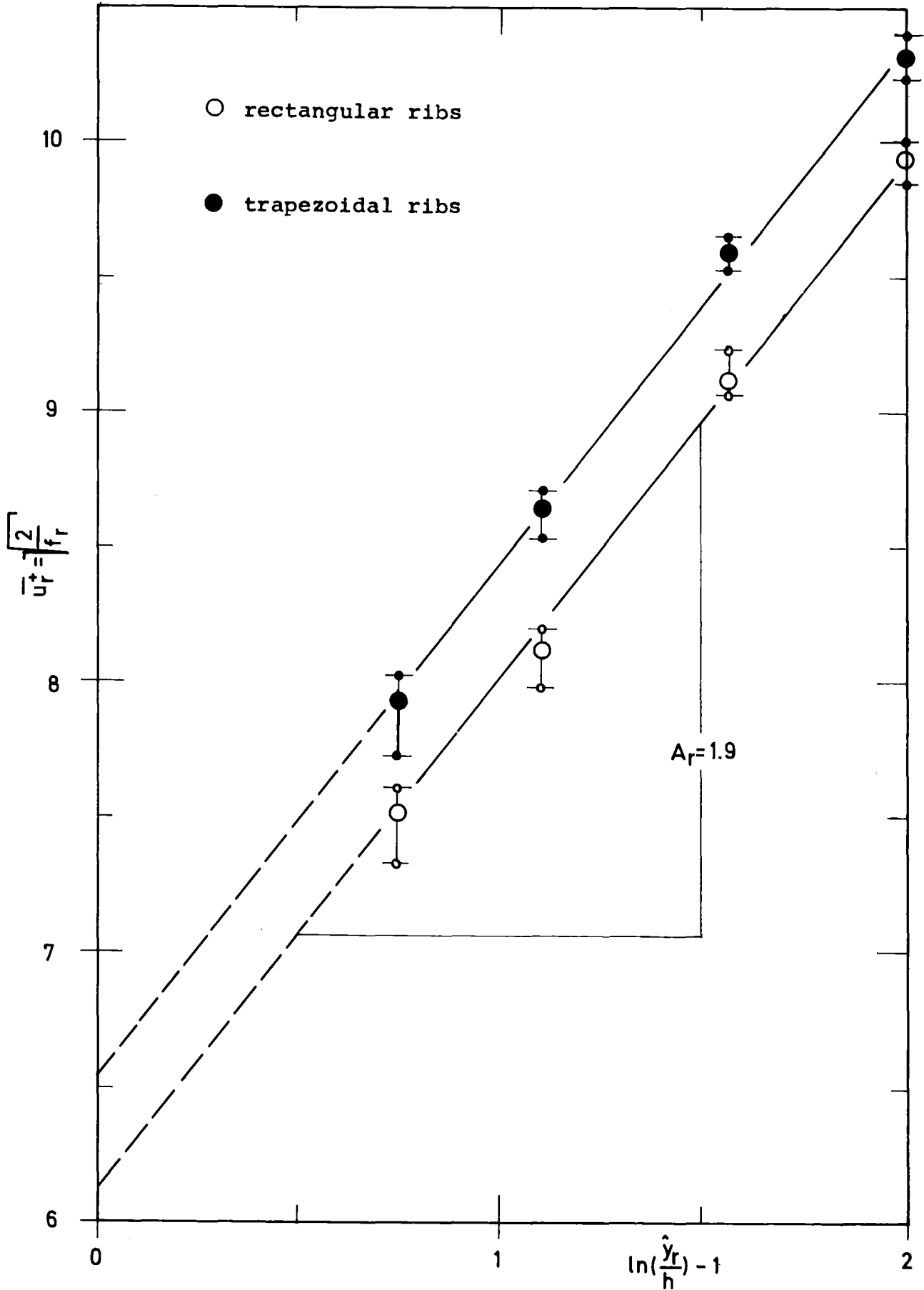


Fig.24: The friction factor of the rough zone f_r as function of $\ln(\hat{y}_r/h) - 1$, ($\epsilon = \epsilon_{vol}$).

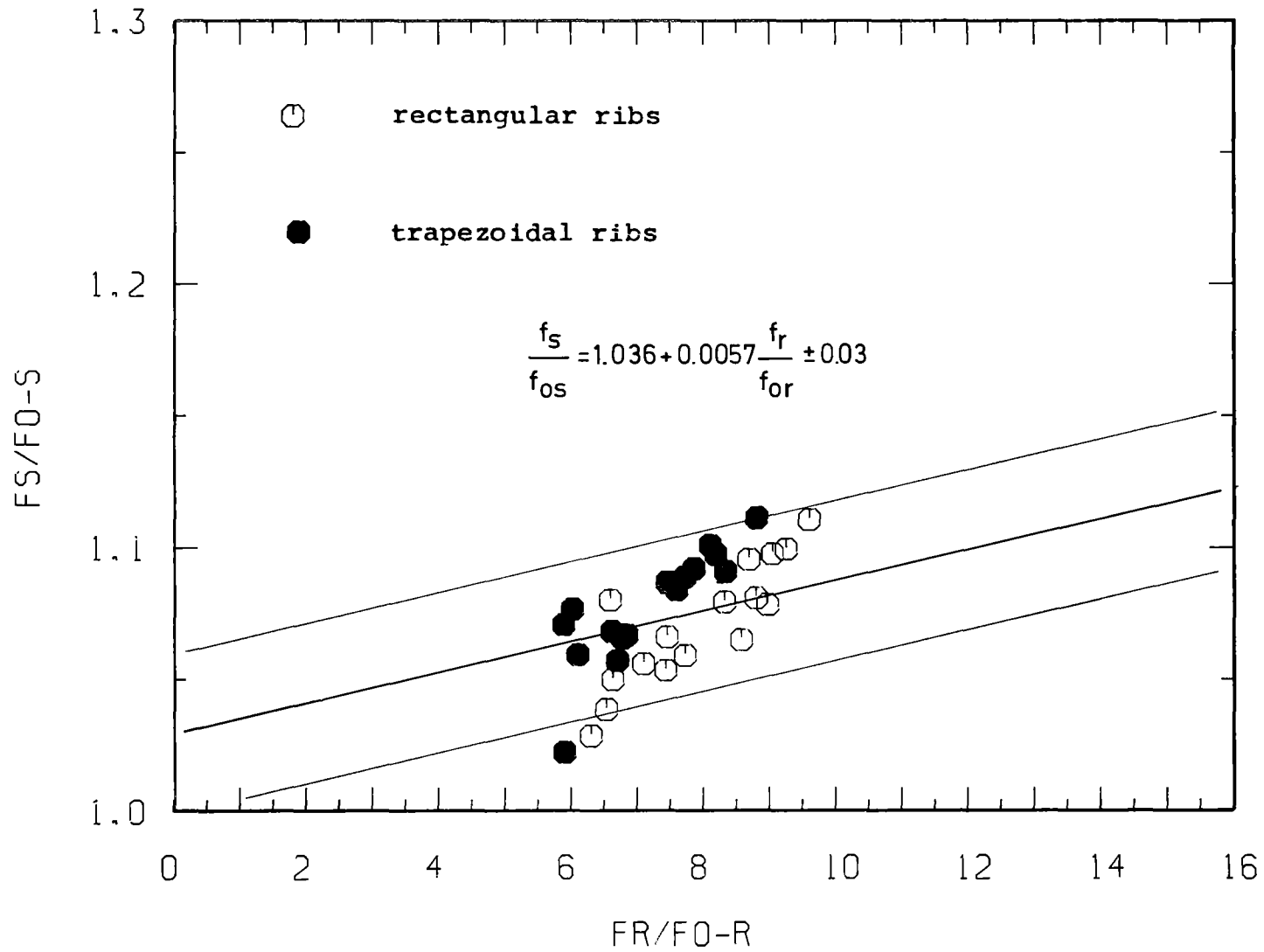


Fig.25: Variation of the friction factor of the smooth zone f_s with different friction factor of the rough zone f_r , ($\epsilon = \epsilon_{vol}$).

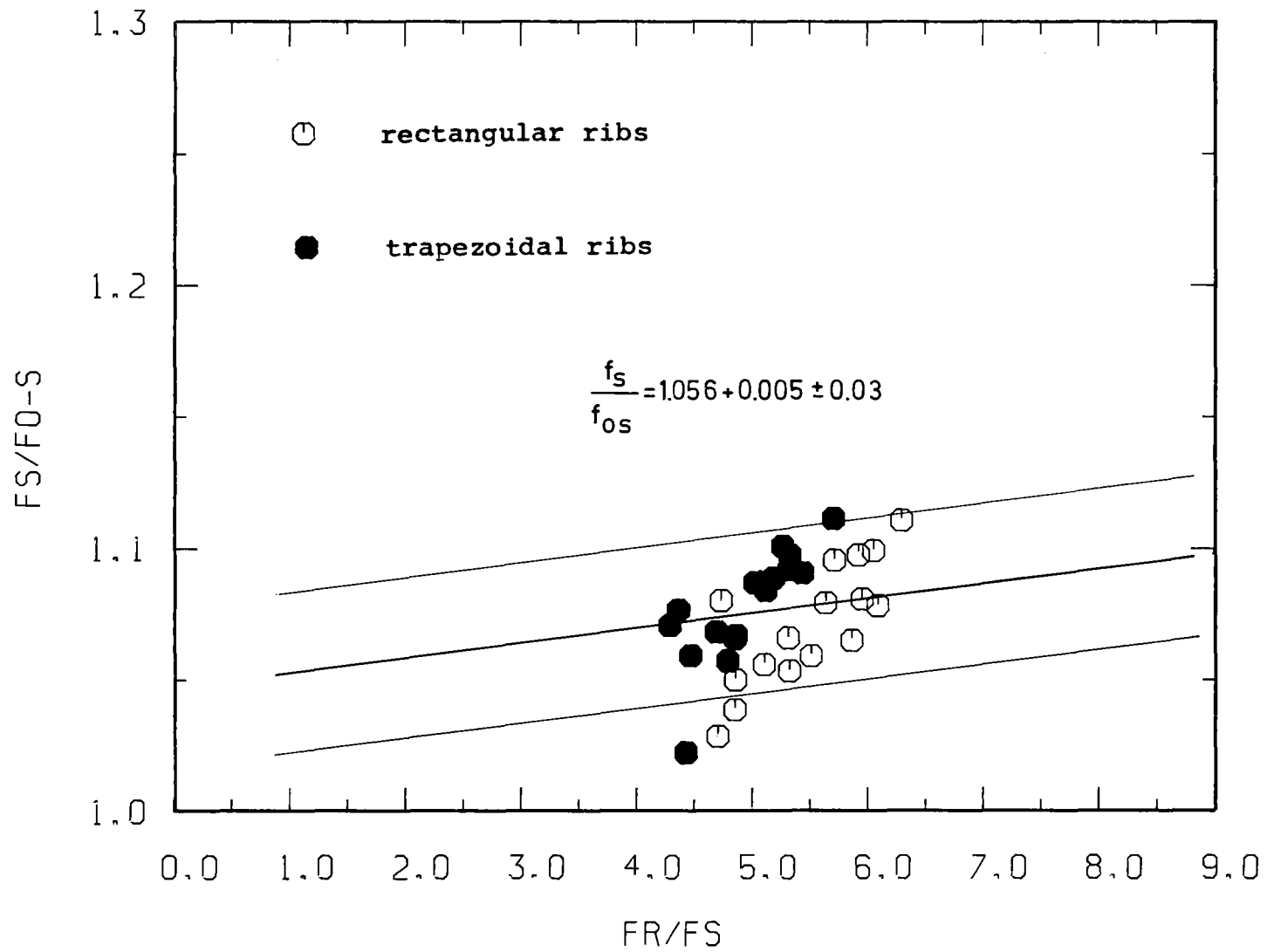


Fig.26: Variation of the friction factor of the smooth zone f_s with the friction factor ratio f_r/f_s , ($\epsilon = \epsilon_{vol}$).

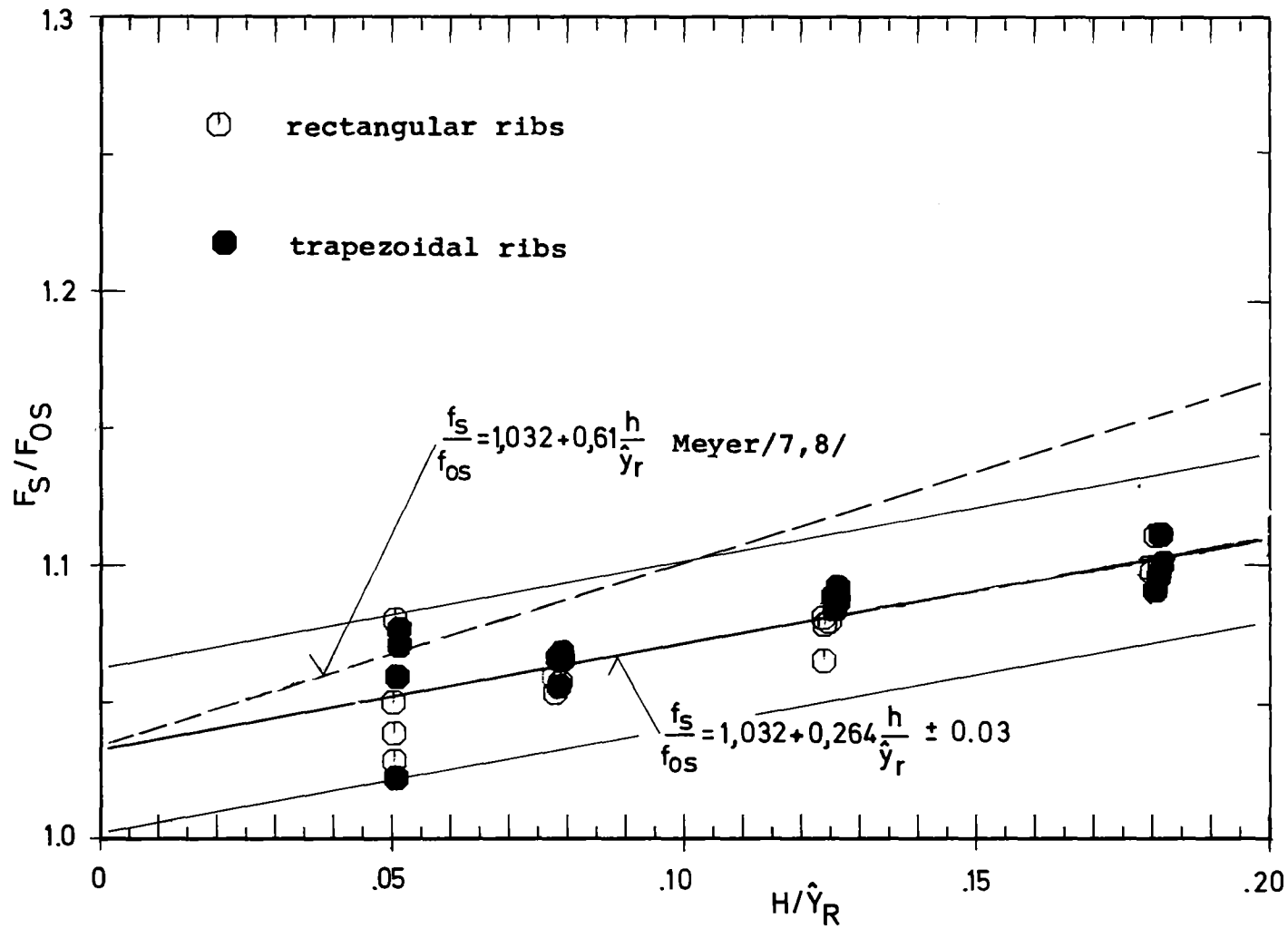


Fig.27: Variation of the friction factor of the smooth zone f_s with relative length of rough zone \hat{y}_R , ($\epsilon = \epsilon_{vol}$).

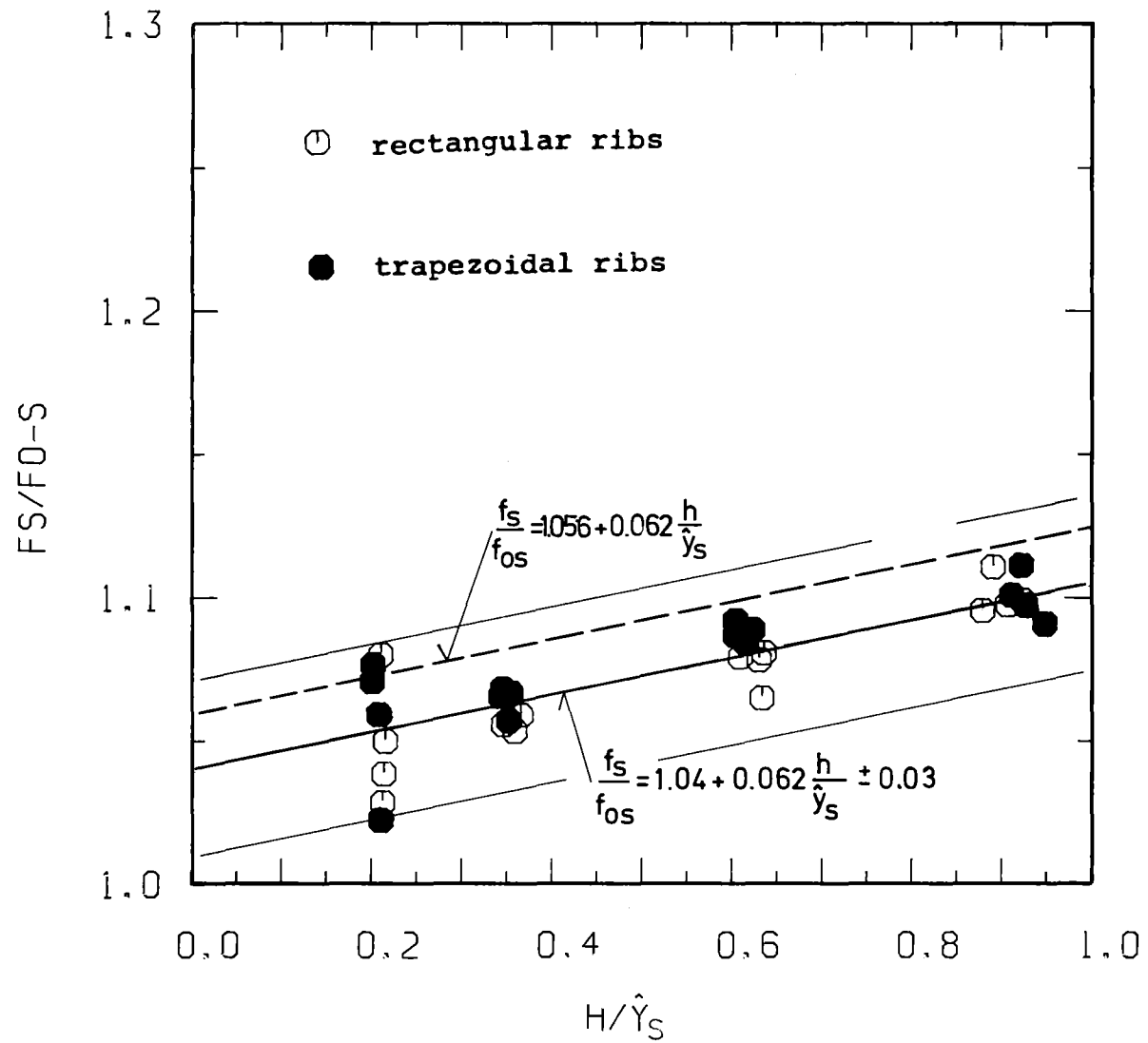


Fig.28: Variation of the friction factor of the smooth zone f_s with relative length of smooth zone \hat{y}_s .

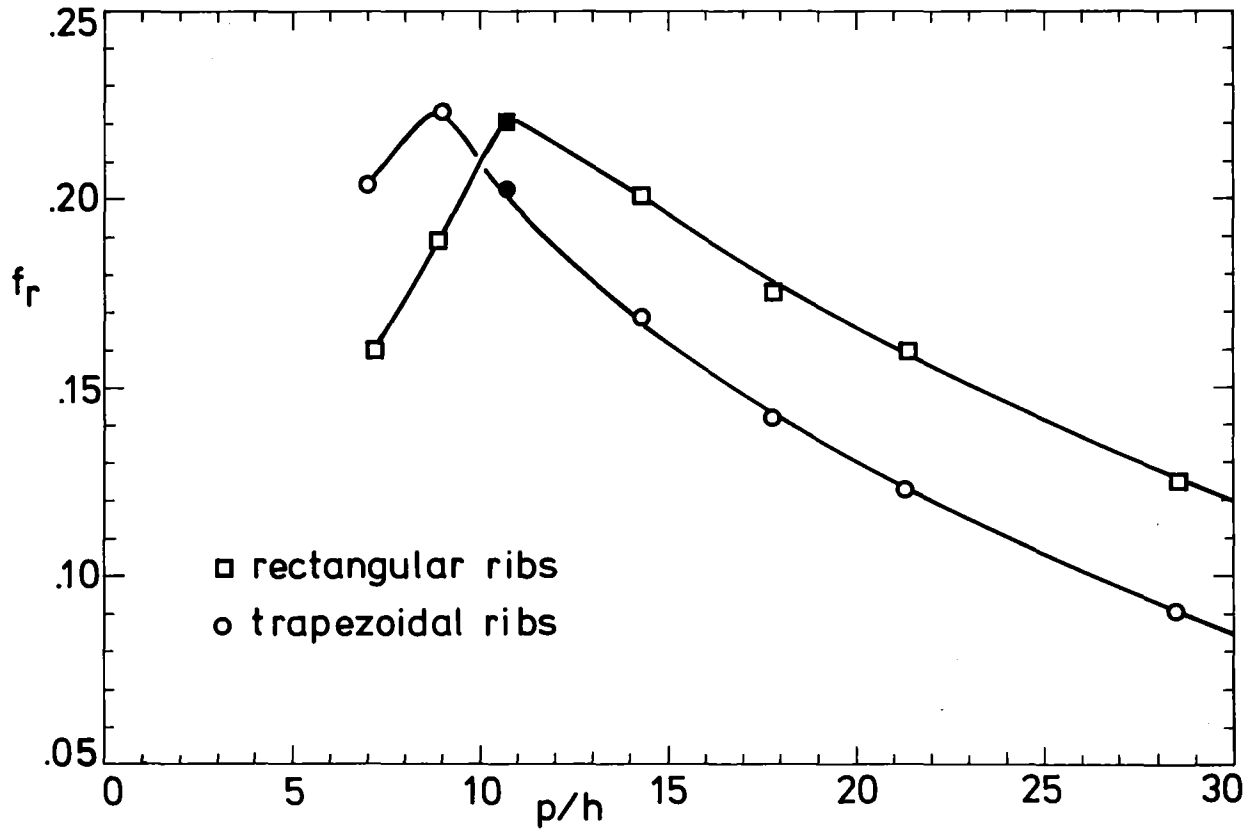


Fig.29: Variation of the friction factor f_r with the pitch-to-height ratio p/h .